*Chem Biol Drug Des 2010;* **75:** 51–67

Research Article



doi: 10.1111/j.1747-0285.2009.00914.x

# Synthesis, Properties, and Applications of Diazotrifluropropanoyl-Containing Photoactive Analogs of Farnesyl Diphosphate Containing Modified Linkages for Enhanced Stability

**Marisa L. Hovlid[1], Rebecca L. Edelstein[1], Olivier Henry[1], Joshua Ochocki[1], Amanda DeGraw[1], Stepan Lenevich[1], Trista Talbot[1], Victor G. Young[1], Alan W. Hruza[2], Fernando Lopez-Gallego[3], Nicholas P. Labello[4], Corey L. Strickland[2], Claudia Schmidt-Dannert[3] and Mark D. Distefano[1,*]**

[1]*Department of Chemistry, University of Minnesota, Minneapolis, MN 55455, USA*
[2]*Department of Structural Chemistry, Schering-Plough Research Institute, Kenilworth, NJ 0703, USA*
[3]*Department of Biochemistry, Molecular Biology and Biophysics, University of Minnesota, St. Paul, MN 55108, USA*
[4]*Minnesota Supercomputing Institute, University of Minnesota, Minneapolis, MN 55455, USA*
**Corresponding Author: Mark D. Distefano, diste001@umn.edu*

**Photoactive analogs of farnesyl diphosphate (FPP) are useful probes in studies of enzymes that employ this molecule as a substrate. Here, we describe the preparation and properties of two new FPP analogs that contain diazotrifluoropropanoyl photophores linked to geranyl diphosphate via amide or ester linkages. The amide-linked analog (3) was synthesized in $^{32}$P-labeled form from geraniol in seven steps. Experiments with *Saccharomyces cerevisiae* protein farnesyltransferase (ScPFTase) showed that 3 is an alternative substrate for the enzyme. Photolysis experiments with [$^{32}$P]3 demonstrate that this compound labels the β-subunits of both farnesyltransferase and geranylgeranyltransferase (types 1 and 2). However, the amide-linked probe 3 undergoes a rearrangement to a photochemically unreactive isomeric triazolone upon long term storage making it inconvenient to use. To address this stability issue, the ester-linked analog 4 was prepared in six steps from geraniol. Computational analysis and X-ray crystallographic studies suggest that 4 binds to protein farnesyl transferase (PFTase) in a similar fashion as FPP. Compound 4 is also an alternative substrate for PFTase, and a $^{32}$P-labeled form selectively photocrosslinks the β-subunit of ScPFTase as well as *E. coli* farnesyldiphosphate synthase and a germacrene-producing sesquiterpene synthase from *Nostoc sp. strain PCC7120* (a cyanobacterial source). Finally, nearly exclusive labeling of ScPFTase in crude *E. coli* extract was observed, suggesting that [$^{32}$P]4 manifests significant selectivity and should hence be useful for identifying novel FPP-utilizing enzymes in crude protein preparations.**

**Key words:** diazotrifluoropropanoyl, farnesyl diphosphate, germacrene synthase, photoaffinity labeling, prenyltransferase, protein prenylation, sesquiterpene synthase

**Abbreviations:** BSA, bovine serum albumin; CPK, bovine Corey-Pauling-Koltun; DATFP, diazotrifluoropropanoyl; DEAD, diethyl azodicarboxylate; DEPT, Distortionless Enhancement by Polarization Transfer; DFT, Density functional theory; DTT, dithiothreitol; EcFPPSase, *E. coli* farnesyl diphosphate synthase; EDTA, ethylenediaminetetraacetic acid; ESI-MS, electrospray ionization mass spectrometry; ESI-TOF, High resolution time of flight; EtOAc, Ethyl acetate; FAB-MS, fast atom bombardment mass spectrometry; FPP, farnesyl diphosphate; FT-IR, Fourier transform infrared spectrum; GGPP, geranylgeranyl diphosphate; HPLC, high performance liquid chromatography; HR-ESI-MS, High resolution electrospray ionization mass spectrometry; HR-FAB-MS, High resolution fast atom bombardment mass spectrometry; HsPGGTase I, *H. sapiens* protein geranylgeranyltransferase type 1; NMR, nuclear magnetic resonance; NoSTSase, *Nostoc sp. strain PCC7120* sesquiterpene synthase; PFTase, protein farnesyl transferase; PPTS, pyridinium *p*-toluenesulfonate; QM-MM, quantum mechanics molecular mechanics; RnPGGTase II, *R. norvegicus* protein geranylgeranyltransferase type 2; RnPFTase, *R. norvegicus* protein farnesyltransferase; *ScPFTase, S. cerevisiae* protein farnesyltransferase; SDS–PAGE, sodium dodecylsulfate polyacrylamide gel electrophoresis; THF, Tetrahydrofuran; THP, Tetrahydropyran.

Received 13 August 2009, revised 23 October 2009 and accepted for publication 24 October 2009

Farnesyl diphosphate (FPP, **1**, see Figure 1) is an important metabolite in the biosynthesis of a variety of molecules including sesquiterpenes (1,2) and the side chains of a number of cofactors;(3) FPP also serves as the source of prenyl groups that are appended to proteins (4). Photoactive analogs of FPP have been useful in

***Editor's invited manuscript to celebrate the 4th Anniversary of Chemical Biology & Drug Design.***

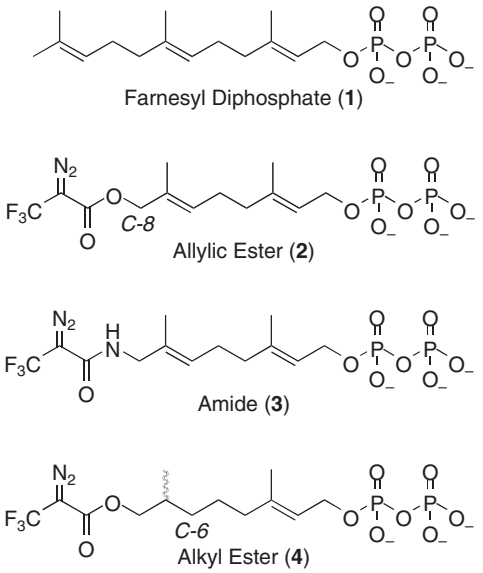


**Figure 1:** Farnesyl diphosphate and related diazotrifluoropropanoyl-containing photoprobes.

identifying proteins and enzymes that use this molecule as a substrate. Hence, a variety of photocrosslinking groups have been used to prepare FPP analogs for use in such experiments including diazotrifluropropionates (DATFP) (5–12), benzophenones (13–22), and aryl azides (23,24). While DATFP-based probes do suffer from the disadvantage that they require activation at lower wavelengths than benzophenone-containing and aryl azide-containing reagents, they also have the advantage that they are intrinsically smaller than most other types of photoactive moieties; in particular, a DATFP group is an excellent mimic of a single isoprene unit. For that reason, Baba and Allen synthesized compound **2** and initially employed it in studies with FPP synthase (6–8). In subsequent years, this compound has been used extensively by a number of researchers in experiments with protein prenyltransferases (5,9,11,25).

One feature of compound **2** that makes it suboptimal for photoaffinity labeling experiments is the ester linkage that connects the photoactive DATFP moiety with the isoprenoid skeleton. Because of the allylic nature of this ester, cleavage between the two parts of the molecule can occur by nucleophilic addition to either the ester carbonyl or the allylic position (C-8). This causes problems in the synthesis but more critically, it can result in loss of the radioactive label (usually present at C-1) in subsequent crosslinking experiments. To circumvent this problem, we decided to explore the synthesis and use of DATFP-containing analogs that incorporate more stable linkages between the crosslinking group and isoprenoid. In this paper, we first describe the preparation and use of an amide-linked DATFP analog (**3**); the design of that compound is based on earlier work with amide-linked benzophenone-containing probes (19). While this new compound functions as an alternative substrate of *Saccharomyces cerevisiae* protein farnesyltransferase (ScPFTase) and selectively labels the $\beta$-subunit of all three known protein prenyltransferases, its diazo amide moiety undergoes a rearrangement to a photochemically inert triazoline over time in aqueous solution. This property limits the utility of this probe. Next, we describe the synthesis of **4**, an analog based on a 6,7 dihydrogeranyl framework that replaces the allylic ester present in **2** with an alkyl ester; that design is based on earlier work with azide-containing alternative substrates for ScPFTase (26,27). Computational analysis and X-ray crystallographic studies suggest that **4** binds to protein farnesyl transferase (PFTase) in a similar fashion as FPP. Compound **4** is also an alternative substrate for ScPFTase and labels a number of FPP-utilizing enzymes including protein farnesyltransferase, farnesyl diphosphate synthase and a sesquiterpene cyclase. Of particular significance, photolysis of crude *E. coli* extracts expressing ScPFTase, in the presence of **4**, results in labeling of the enzyme suggesting that this probe should be useful for identifying other FPP-utilizing enzymes present in complex protein mixtures.

## Materials and Methods

### *General*

All *trans*-geraniol, dimethylallyl alcohol, *t*-butyl hydroperoxide, $H_2SeO_3$, salicylic acid, hydrazine monohydrate, toluene sulfonic acid, and trichloroacetonitrile were obtained from Aldrich (St. Lous, MO). All synthetic reactions were performed at room temperature in open air, with magnetic stirring unless noted otherwise. TLC analysis was performed on precoated (250 $\mu$m) silica gel 60 F-254 plates from Merck (Whitehouse Station, NJ), and the plates were visualized by UV light at 254 nm or $KMnO_4$ staining. Flash chromatography silica gel (60–120 mesh) was obtained from Mallickrodt Baker Inc., Paris, KY, USA. Dowex 50W-X8 resin and silver staining kits were obtained from Bio-Rad (Hercules, CA), Sep-Pak columns were purchased from Waters (Millford, MA), and Amplify was from Amersham Life Science Amersham (Piscataway, NJ). $[^{32}P]H_3PO_4$ (specific activity 8500–9120 Ci/mmol) was purchased from DuPont NEN Dupont NEN (Boston, MA). $CH_2Cl_2$ and $CH_3CN$ were dried with an M. Braun solvent purification system. Deuterated solvents were used as obtained from Cambridge Isotope Laboratories Inc. Cambridge Isotope (Andover, MA). $^1$H-NMR spectra were obtained at 300 MHz and $^{13}$C-NMR at 75 MHz. All nuclear magnetic resonance (NMR) spectra were acquired on Varian (Palo Alto, CA) instruments at 25 °C. Chemical shifts are reported in ppm with *J* values reported in Hz. IR readings were taken using NaCl polished plates. HPLC was performed on a Beckman 127/166 instrument equipped with a Linear Instruments LC305 fluorescence detector. Phosphor imaging analysis was performed with a Molecular Dynamics 445 SI Phosphor imager. *N*-dansyl-GCVIA was synthesized by Dr. Dan Mullen in the Department of Chemistry, University of Minnesota. ScPFTase (21), *H. sapiens* protein geranylgeranyltransferase type 1 (HsPGGTase I), *E. coli* farnesyl diphosphate synthase (EcFPPSase) (28), and *Nostoc sp. strain PCC7120* sesquiterpene synthase (NoSTSase) (29) were purified as previously described. *R. norvegicus* protein geranylgeranyltransferase type 2 (RnPGGTase II) was a generous gift from Dr. Miguel Seabra (Imperial College, London).

### *(E,E)*-8-*N*-(2-Diazo-3,3,3-trifluoropropionamido)-3,7-dimethyl-2,6-octadienyl-1-diphosphate (3).

Alcohol **9** (3.1 mg, 10 $\mu$mol) was reacted with anhydrous $H_3PO_4$ (2.0 mg, 20 $\mu$mol, prepared by lyophilization over $P_2O_5$) in $CH_3CN$ (255 $\mu$L) containing 25% (v/v) $CCl_3CN$ and triethylamine (40 $\mu$mol)

for 2 h at rt under $N_2$. The volatile components were then evaporated, and the resulting residue was partially purified by reversed-phase chromatography on a Sep-Pak $C_{18}$ cartridge with an $NH_4HCO_3$/$CH_3CN$ step gradient from 0–100% $CH_3CN$; pure product eluted at 25% $CH_3CN$. The fractions containing the desired pyrophosphate product were concentrated and redissolved in 25 mM $NH_4HCO_3$, and the final concentration was determined by UV absorbance (236 nm, extinction coefficient = 14 000 per cm/M) (30). Diphosphate **3** was obtained in 8% yield, and the purity was determined to be 93% diphosphate, 7% monophosphate by reversed-phase HPLC analysis. $^1$H-NMR (300 MHz, $D_2O$, pH 8.0): $\delta$ = 1.53 (s, 3H), 1.56 (s, 3H), 2.00–2.05 (m, 4H), 3.65 (s, 2H), 4.13 (t, 2H, $J$ = 6.0), 5.26–5.30 (m, 2H); High resolution fast atom bombardment mass spectrometry (HR-FAB-MS) calcd for $C_{13}H_{10}N_3O_8P_2F_3Na$ $[M+Na]^+$ 488.0576, found 488.0609

### *(E,E)*-[α,β(*n*)$^{32}$P]-8-*N*-(2-Diazo-3,3,3-trifluoropropionamido)-3,7-dimethyl-2,6-octadienyl-1-diphosphate ([$^{32}$P]3)

Alcohol **9** (2.0 mg, 6.3 μmol) was reacted with anhydrous $[^{32}P]H_3PO_4$ (1.2 mg, 13 μmol) prepared as previously described in $CH_3CN$ (200 μL) containing 20% (v/v) $CCl_3CN$ and triethylamine (2.5 mg, 26 μmol) for 2 h (31). The volatile components were then evaporated, and the resulting residue was purified using a reversed-phase Sep-Pak $C_{18}$ cartridge with an $NH_4HCO_3$/$CH_3CN$ step gradient. The product ([$^{32}$P]**3**) eluted from the Sep Pak cartridge in fractions containing 20% and 25% $CH_3CN$. After evaporation and redissolving in 25 mM $NH_4HCO_3$, [$^{32}$P]**3** (specific activity: 1.25 Ci/mmol) was obtained, giving a 7% yield. The radiochemical purity was determined to be 40%, as assessed by thin layer chromatography in isopropanol/$NH_4OH$/$H_2O$ (6:3:1, v/v/v), followed by phosphor imaging analysis.

### (*E*)-8-*O*-(2-Diazo-3,3,3-trifluoropropanoyloxy)-3,7-dimethyl-2-octenyl-1-diphosphate (4)

Anhydrous phosphoric acid was prepared by lyophilization of a solution of 1% $H_3PO_4$ (v/v) (3.8 mL, 0.64 mmol). To that residue was added $CH_3CN$ (1.6 mL), and $Et_3N$ (180 μL, 1.3 mmol) followed by compound **17** (100 mg, 0.32 mmol), dissolved in 3.2 mL of a solution of $CCl_3CN$ in $CH_3CN$ (20%, v/v). The reaction was allowed to proceed in the dark under an $N_2$ atmosphere with magnetic stirring for 2 h. The solvent was then removed by rotory evaporation, and the residue was redissolved in 10 mL of 25 mM $NH_4HCO_3$. The product was purified by reversed-phase HPLC with buffer A (25 mM $NH_4OH$) and buffer B ($CH_3CN$) over seven injections, using a linear gradient from 0–35% buffer B over 35 min. Samples (2.0 mL) were injected into a 5 mL loop, onto a Phenomex Luna $C_{18}$ semi-preparative column (250 × 10 mm). Monitoring at a wavelength of 236 nm, the desired product eluted at 22–26% solvent B. The product-containing fractions were lyophilized to yield 23 mg (16%) of a white powder. $^1$H-NMR (300 MHz, $D_2O$) $\delta$ 0.77 (d, $J$ = 6.6 Hz, 3H), 1.05–1.40 (m, 6H), 1.55 (s, 3H), 1.63–1.80 (m, 1H), 1.90 (t, $J$ = 7.5 Hz, 2H), 3.99 (t, $J$ = 6.9 Hz, 2H), 4.14 (t, $J$ = 6.3 Hz, 2H), 5.31 (t, $J$ = 6.0 Hz, 1H); $^{31}$P-NMR (121 MHz, $CDCl_3$) −5.93 (d, $J$ = 22.0 Hz, 1P), −0.91 (d, $J$ = 22.0 Hz, 1P); HR-MS High resolution time of flight (ESI-TOF) calcd for $C_{13}H_{20}F_3N_2O_9P_2$ $[M-H]^-$ 467.0596, found 467.0594.

### (*E*)-[α,β(*n*)$^{32}$*P*]-8-*O*-(2-Diazo-3,3,3-trifluoropropanoyloxy)-3,7-dimethyl-2-octeny-1-diphosphate ([$^{32}$P]4)

Radiolabeled [$^{32}$P]**4** was synthesized using a procedure similar to that described for unlabeled **4**. Briefly, a solution of 1% $H_3PO_4$ (v/v) (110 μL, 20 μmol) was prepared in a 10 mL round bottom flask and lyophilized overnight as previously described. Compound **17** (3.1 mg, 10 μmol) was dissolved in 50 μL $CH_3CN$ and added to the reaction flask containing the anhydrous $H_3PO_4$. To this solution, a mixture of $CH_3CN$/$CCl_3CN$ 20% (v/v) (200 μL) was added, followed by $Et_3N$ (5.6 μL). The reaction was stirred in the dark under an Ar atmosphere for 2 h followed by evaporation under a stream of $N_2$ (g) to yield a yellow residue. The resulting material was then dissolved in 25 mM $NH_4HCO_3$ (5 mL) and applied to a reversed-phase Sep-Pak cartridge equilibrated in 25 mM $NH_4HCO_3$. The column was eluted with a step gradient of $CH_3CN$ (10% steps, 4 × 1.0 mL fractions per step), and the composition of the fractions was determined by TLC (i-PrOH/$NH_4OH$/$H_2O$, 6:3:1 v/v/v) followed by phosphor imaging analysis. After evaporation of the product-containing fractions (30% $CH_3CN$) and redissolving in 25 mM $NH_4HCO_3$, [$^{32}$P]**4** (specific activity: 275 Ci/mol) was obtained. The radiochemical purity was determined to be 24%, as assessed by TLC (i-PrOH/$NH_4OH$/$H_2O$, 6:3:1, v/v/v), followed by phosphor imaging analysis; Impurities that were present include the corresponding monophosphate (36%), the triphosphate (11%), and inorganic phosphate (9%). The remaining 20% is likely a dimer formed by condensation of two monophosphates. The concentration of [$^{32}$P]**4** was determined by UV spectroscopy using the extinction coefficient ($\varepsilon_{236}$ = 14 000 per cm/M) previously reported for the diazoester fragment (30).

### (*E,E*)-8-*N*-(2-Diazo-3,3,3-trifluoropropionamido)-3,7-dimethyl-1-tetrahydropyranyl-2,6-octadiene (8)

The amine **6** was prepared by reacting phthalimide **5** (300 mg, 0.78 mmol) with $NH_2NH_2$•$H_2O$ (62 mg, 1.2 mmol) in EtOH (10 mL) at rt for 16 h. The reaction was filtered and used directly in the next step of the synthesis without further purification. Amide **8** was prepared by reacting crude **6** (110 mg, 0.43 mmol) with **7** (100 mg, 0.58 mmol) in dry pyridine (0.5 mL) at 0 °C. The reaction was stirred in the dark for 30 min under $N_2$, followed by an additional 2 h at rt. It was then concentrated *in vacuo*, redissolved in Ethyl acetate (EtOAc), and washed sequentially with 0.10 N HCl, 1.0 M $NaHCO_3$, and aqueous saturated NaCl. The organic layer was dried over $MgSO_4$, filtered, concentrated under reduced pressure, and the crude product was purified by flash chromatography on silica (toluene/EtOAc, 4:1, v/v), giving **8** in 18% yield (30 mg, 77 μmol). $R_f$ = 0.44 (silica gel, toluene/EtOAc, 4:1, v/v); $^1$H-NMR (500 MHz, $CDCl_3$) $\delta$ 1.52–1.81 (m, 6H), 1.62 (s, 3H), 1.67 (s, 3H), 2.05–2.09 (m, 2H), 2.13–2.18 (m, 2H), 3.49–3.53 (m, 1H), 3.85–3.91 (m, 1H), 3.88 (d, 2 H, $J$ = 8.5), 3.98–4.04 (m, 1H), 4.21–4.27 (m, 1H), 4.61–4.63 (m, 1H), 5.28–5.38 (m, 2H); $^{13}$C-NMR (75.4 MHz, $CDCl_3$, Distortionless Enhancement by Polarization Transfer (DEPT)) $\delta$ 14.38, 16.39 (primary C); 19.62, 25.49, 25.99, 30.71, 39.08, 47.45, 62.31, 63.64 (secondary C); 97.92, 121.03, 126.95 (tertiary C); 122.22, 125.79, 131.20, 139.56, 158.94 (quaternary C); $^{19}$F-NMR (282.2 MHz, $CDCl_3$) $\delta$ −55.77.

### (*E,E*)-8-*N*-(2-Diazo-3,3,3-trifluoropropionamido)-3,7-dimethyl-2,6-octadien-1-ol (9)

Alcohol **9** was prepared by reacting protected DATFP ester (**8**, 50 mg, 0.13 mmol) with TsOH (1.3 mg, 6.9 $\mu$mol) in MeOH (13 mL) in the dark at rt for 20 h. The reaction mixture was then concentrated under reduced pressure and purified by flash chromatography on silica (toluene/EtOAc 4:1, v/v) giving the pure product in 67% yield (26 mg, 85 $\mu$mol). $R_f$ = 0.15 (silica gel, toluene/EtOAc, 4:1, v/v); $^1$H-NMR (300 MHz, $CDCl_3$) $\delta$ 1.62 (s, 3H), 1.66 (s, 3H), 2.04–2.09 (m, 2H), 2.13–2.18 (m, 2H), 3.87 (d, 2H, $J$ = 5.7), 4.14 (d, 2H, $J$ = 6.9), 5.25–5.30 (m, 1H), 5.36–5.42 (m, 1H), 5.45 (broad s, 1H); $^{13}$C-NMR (75.4 MHz, $CDCl_3$, DEPT): $\delta$ 14.38, 16.12 (primary C); 25.74, 38.94, 47.41, 59.31 (secondary C); 124.01, 126.50 (tertiary C); 122.22, 125.79, 131.19, 138.78, 159.03 (quaternary C); $^{19}$F-NMR (282.2 MHz, $CDCl_3$) $\delta$ −55.77; HR-FAB-MS calcd for $C_{13}H_{18}N_3O_2F_3Na$ $[M+Na]^+$ 328.1249, found 328.1259.

### 2,2′-((2*E*,6*E*)-2,6-dimethylocta-2,6-diene-1,8-diyl)diisoindoline-1,3-dione (10)

Compound **5** (150 mg, 0.40 mmol) and pyridinium *p*-toluenesulfonate (PPTS) (98 mg, 0.4 mmol) were dissolved in EtOH (4.8 mL) and stirred at 55 °C for 4 h. The solvent was removed *in vacuo*, redissolved in $Et_2O$ (5 mL) and washed with half-saturated brine to remove the catalyst. The ether solution was dried over $Na_2SO_4$ and evaporated to yield 83 mg of the desired deprotected alcohol in (70% yield). $R_f$ = 0.30 (silica gel, hexane/EtOAC, 5:2, v/v); $^1$H NMR (300 MHz, $CDCl_3$): $\delta$ 1.60 (s, 3H), 1.63 (s, 3H), 2.04–2.08 (m, 2H), 2.11–2.19 (m, 2H), 4.10 (d, 2H, $J$ = 6.3), 4.17 (s, 2H), 5.24–5.35 (m, 2H), 7.68–7.75 (m, 2H), 7.82–7.87 (m, 2H); High resolution electrospray ionization mass spectrometry (HR-ESI-MS) calcd for $C_{18}H_{21}NaNO_3$ $[M+Na]^+$ 322.1419, found 322.1397. The previously mentioned deprotected alcohol (80 mg, 0.27 mmol) was combined with phthalimide (45 mg, 0.27 mmol) and $PPh_3$ (68 mg, 0.27 mmol) in 2.2 mL Tetrahydrofuran (THF). To the stirred solution was added diethyl azodicarboxylate (DEAD) (6 $\mu$L, 0.27 mmol) in 0.6 mL THF dropwise over 30 min. The reaction mixture was stirred for 18 h at rt followed by a second addition of $PPh_3$ (42 mg, 0.15 mmol) and DEAD (3.0 $\mu$L, 0.15 mmol). The reaction was stirred overnight at rt and quenched with hexane (5.0 mL) to precipitate the reaction byproducts. The filtrate was evaporated, and the residue was purified by flash chromatography (silica gel, hexane/EtOAC, 5:2, v/v) to yield compound **10** (63 mg, 54%) as a white solid. Crystallization of the product was achieved by adding 5.5 mL $CH_3OH$ and heating in an oil bath with swirling until the solid was completely dissolved. The flask was removed from the heat and left undisturbed, to cool to rt. Crystals formed over a period of 4 h. $R_f$ = 0.50, silica gel, hexane/EtOAC, 5:2, v/v; $^1$H NMR (300 MHz, $CDCl_3$): $\delta$ 1.59 (s, 6H), 1.98–2.03 (m, 2H), 2.07–2.12 (2H), 4.16 (s, 2H), 4.26 (d, 2H, $J$ = 7.2), 5.24 (t, 1H, $J$ = 6.3), 5.32 (t, 1H, $J$ = 6.3), 7.69–7.33 (m, 4H), 7.83–7.87 (m, 4H); HR-ESI-MS calcd for $C_{26}H_{24}Na_2N_2O_4$ $[M+Na]^+$ 451.1634, found 451.1648.

### (*E*)-8-*O*-(2-Diazo-3,3,3-trifluoropropanoyloxy)-3,7-dimethyl-1-*O*-tetrahydropyranyl-2-octene (16)

Pyridine (3 mL) was added to alcohol **15** (100 mg, 0.39 mmol), and the reaction flask was sealed with a rubber septum. 2-diazo-3,3,3-trifluoropropanoyl chloride (DATFP-Cl, **7**, 85 mg, 0.49 mmol) was then added, and the mixture was cooled to 0 °C and allowed to react with stirring, in the dark, for 30 min followed by an additional 2 h at rt. The solvent (pyridine) was removed *in vacuo,* and the resulting residue dissolved in $Et_2O$ and washed sequentially with 0.10 M HCl, 1.0 M $NaHCO_3$, and aqueous saturated NaCl. The organic layer was dried over $MgSO_4$, filtered, concentrated under reduced pressure, and the resulting crude product was purified by flash chromatography (hexanes: EtOAc, 6:1) affording compound **16** in 88% yield. $^1$H-NMR (300 MHz, $CDCl_3$) $\delta$ 0.95 (d, 2H, $J$ = 6.6 Hz), 1.12–1.64 (m, 12H), 1.73 (s, 3H), 1.80 (m, 2H), 2.03 (t, 2H, $J$ = 7.5 Hz), 3.52 (m, 1H), 3.91 (m, 1H), 4.05 (m, 2H), 4.16 (dd, 1H, $J_1$ = 5.7 Hz, $J_2$ = 10 Hz), 4.24 (dd, 1H, $J_1$ = 6.6 Hz, $J_2$ = 12 Hz), 4.64 (t, 1H, $J$ = 4.2 Hz), 5.37 (t, 1H, $J$ = 6.9 Hz); $^{13}$C-NMR (75 MHz, $CDCl_3$) $\delta$ 16.33, 16.73, 19.69, 24.77, 25.55, 30.77, 32.58, 32.76, 39.69, 62.38, 63.71, 70.80, 97.97, 120.88, 121.73, 124.54, 140.04, 161.10; $^{19}$F-NMR (282 MHz, $CDCl_3$) $\delta$ −58.02 (s, 3F); Fourier transform infrared spectrum (FT-IR) (neat) 1320 (vs), 1352 (vs), 1394 (s), 1732 (vs), 2136 (vs), 2344 (w), 2361 (w), 2869 (s), 2939 (vs) per cm; HR-MS (ESI-TOF) calcd for $C_{18}H_{27}F_3N_2NaO_4$ $[M+Na]^+$ 483.2441, found 483.2444.

### (*E*)-8-*O*-(2-Diazo-3,3,3-trifluoropropanoyloxy)-3,7-dimethyl-2-octen-1-ol (17)

Alcohol **16** (135 mg, 0.34 mmol) was dissolved in 10 mL of absolute EtOH. After adding PPTS (12 mg, 50 $\mu$mol), the flask was sealed with a rubber septum and stirred in the dark for 6 h at 60 °C. The product was purified by flash chromatography (hexanes: EtOAc, 5:1, v/v) and obtained in 90% yield. $^1$H-NMR (300 MHz, $CDCl_3$) $\delta$ 0.95 (d, 3H, $J$ = 6.6 Hz), 1.10–1.56 (m, 6H), 1.67 (s, 3H), 1.81–1.84 (m, 1H), 2.01 (t, 2H, $J$ = 7.8 Hz), 4.05 (dd, 1H, $J_1$ = 6.6 Hz, $J_2$ = 11 Hz), 4.15 (m, 3H), 5.41 (t, 1H, $J$ = 6.9 Hz); $^{13}$C-NMR (75 MHz, $CDCl_3$) $\delta$ 15.83, 16.37, 24.45, 32.26, 32.36, 39.29, 59.04, 70.52, 120.72, 123.43, 124.29, 139.12, 160.97; $^{19}$F-NMR (282 MHz) $\delta$ −58.01 (s, 3F); FT-IR (neat) 1319 (vs), 1351 (vs), 1396 (vs), 1701 (vs), 2135 (vs), 2857 (s), 2925 (vs), 2962 (vs), 3371 (b) per cm; HR-MS (ESI-TOF) calcd for $C_{13}H_{19}F_3N_2NaO_3$ $[M+Na]^+$ 331.1240, found 331.1240.

### 1-(2-Diazo-3,3,3-trifluoropropionyloxy)-3-methyl-2-butene (18)

Dimethylallyl alcohol (100 mg, 1.16 mmol) was dissolved in freshly distilled pyridine (0.5 mL) and stirred until homogenous. A solution of DATFP-Cl (**7**, 239 mg, 1.39 mmol) in pyridine (1.0 mL) was slowly added, and the reaction allowed to proceed at 0 °C in the dark for 2.5 h. The pyridine solvent was removed *in vacuo,* and the product was redissolved in $Et_2O$. The organic layer was then washed sequentially with 0.1 M HCl, 1 M $NaHCO_3$, and brine, dried over $Na_2SO_4$ and concentrated. Purification was accomplished by flash chromatography (hexanes: EtOAc, 3:1) producing 258 mg (64%) of a pale yellow oil. $^1$H-NMR (300 MHz, $CDCl_3$) $\delta$ 1.73 (s, 3H), 1.77 (s, 3H), 3.74 (d, 2H, $J$ = 7.2 Hz), 5.35 (tq, 1H, $J_1$ = 1.5 Hz, 8.7 Hz); $^{13}$C-NMR (75 MHz, $CDCl_3$) $\delta$ 18.04, 25.77, 62.82, 117.76, 121.00, 124.57, 136.14, 160.92; $^{19}$F-NMR (282 MHz, $CDCl_3$) $\delta$ −58.26 (s, 3F); FT-IR (neat) 1313 (vs), 1355 (vs), 1384 (vs), 1448 (m), 1723 (vs), 2137 (vs), 2341 (w), 2360 (w), 2309 (m), 2977 (m) per cm.

### 1-(2-Diazo-3,3,3-trifluoropropionyloxy)-3-methyl-3-butene (19)

Compound **19** was prepared as described for **18** starting from isopentenyl alcohol in 66% yield. $^{1}$H-NMR (300 MHz, $CDCl_3$) $\delta$ 1.76 (s, 3H), 2.39 (t, 2H, $J$ = 6.9 Hz), 4.37 (t, 2H, $J$ = 6.9 Hz), 4.74 (s, 1H), 4.83 (s, 1H); $^{13}$C-NMR (75 MHz, $CDCl_3$) $\delta$ 22.33, 36.74, 64.11, 112.87, 120.92, 124.50, 141.01, 160.85; $^{19}$F-NMR (282 MHz, $CDCl_3$) $\delta$ −58.20 (s, 3F); FT-IR (neat) 1329 (vs), 1344 (vs), 1392 (vs), 1456 (m), 1721 (vs), 2136 (vs), 2256 (m), 2359 (w), 2973 (m), 3081 (m), 3434 (b) per cm.

### Stability studies of 18 and 19

Compound **18** (11 mg, 0.05 mmol) was added to an 8 -inch thin-walled NMR tube and dissolved by the addition of 0.7 mL of mildly acidic solution ($CD_3CN$/$D_2O$ 10%/trifluoroacetic acid (TFA)-*d* 0.1%, v/v/v); a separate NMR tube containing **18** (11 mg, 0.05 mmol) dissolved in a mildly basic solution ($CD_3CN$/$D_2O$ 10%/$ND_4OD$ 0.1%, v/v/v) was also prepared. The samples were then heated directly in the NMR tubes in a 100 °C water bath for 4 h followed by $^{1}$H-NMR analysis. Experiments with **19** in acidic or basic solutions were prepared and analyzed in a similar manner.

### Enzymatic substrate and inhibition studies monitored by fluorescence spectroscopy

The photoactive isoprenoids **3** and **4** were studied as possible substrates for ScPFTase by monitoring the increase in fluorescence of a peptide substrate as it becomes prenylated as previously described (32,33). For experiments with the yeast enzyme, the assay conditions used were 50 mM Tris HCl (pH 7.0), 10 mM $MgCl_2$, 10 $\mu$M $ZnCl_2$, 5.0 mM dithiothreitol (DTT), 0.040% (w/v) *n*-dodecyl-$\beta$-D-maltoside, 2.0 $\mu$M *N*-dansyl-GCVIA, isoprenoid diphosphate (FPP, **3** or **4**, 10 $\mu$M), and ScPFTase (24–92 nM) in a final volume of 500 $\mu$L. For experiments with the mammalian enzyme, similar conditions were employed except that *N*-dansyl-GCVLS (2.4 $\mu$M) was used as a substrate. Enzymatic reactions were initiated by the addition of PFTase and monitored for 300–3000 seconds (340 nm excitation, 505 emission) to determine the rate. For $IC_{50}$ determinations, fluorescence assays were performed in triplicate as described earlier except that reactions contained 2.0 $\mu$M FPP along with **3** or **4** at varying concentrations. The $IC_{50}$ values were determined from a direct plot of rate versus inhibitor concentration.

### Enzymatic substrate studies monitored by HPLC

To confirm the enzymatic modification of *N*-dansyl-GCVIA by **3** and **4**, larger scale reactions (10–15 mL) were performed using the conditions reported for the fluorescence assays described earlier except that the detergent was omitted (detergent is usually included to solubilize the product, not for enzyme activity). In each case, the reaction was initiated with enzyme and incubated at 30 °C for 6–24 h. The reaction mixture was then applied to a Sep Pak cartridge equilibrated in solvent C (5% $CH_3CN$, 95% $H_2O$, 0.1% TFA, v/v/v); product was eluted with solvent B (100% $CH_3CN$, 0.1% TFA, v/v). The fluorescent fractions were concentrated, redissolved in 50% solvent A (100% $H_2O$, 0.1% TFA, v/v) and 50% solvent B, and further purified by reversed-phase HPLC using a Varian Microsorb $C_{18}$ analytical column (250 × 4.6 mm). Elution was performed using a linear gradient from 100% solvent A to 100% solvent B (solvents described earlier) over 40 min with a flow rate of 1 mL/min. The product was collected, lyophilized, and analyzed by MS. In cases where the reaction kinetics were monitored by HPLC, aliquots of 500 $\mu$L were removed at varying time intervals from large scale reactions, flash frozen in $N_2$ (l), and stored at −20 °C prior to analysis. The samples were then thawed and analyzed by reversed-phase HPLC as described earlier.

### Photolabeling of prenyltransferases with [$^{32}$P]DATFP-Amide ([$^{32}$P]3)

For experiments with ScPFTase, purified enzyme (4 $\mu$g) was incubated in 50 mM HEPES (pH 7.5), 1.0 mM DTT, 5.0 mM $MgCl_2$, 10 $\mu$M $ZnCl_2$, 15 $\mu$M [$^{32}$P]**3** (dissolved in 25 mM $NH_4HCO_3$), and 30 $\mu$M FPP (where appropriate, dissolved in 25 mM $NH_4HCO_3$) or the equivalent volume of 25 mM $NH_4HCO_3$ in a final volume of 75 $\mu$L. Samples were irradiated at 254 nm at 4 °C for 3 min in quartz test tubes (10 × 45 mm) using a UV Rayonet mini-reactor equipped with 4 RPR-2540 Å lamps and a circulating platform. The samples were heated to 70 °C for 5 min in loading buffer (4% SDS, 12% glycerol (w/v), 50 mM Tris, 2% mercaptoethanol (v/v), 0.01% Serva blue G, pH 6.8) and analyzed by SDS–PAGE with a 10% Tris-tricine gel. The gel was fixed by slow shaking in isopropanol/$H_2O$/acetic acid (25:65:10, v/v/v) for 20 min. It was then exposed to a phosphor imaging screen for 3 h, followed by silver staining. Experiments with HsPGGTase were performed as described earlier except that geranylgeranyl diphosphate (30 $\mu$M final concentration) was used instead of FPP to demonstrate substrate protection. Experiments with RnPGGTase II were also performed as described earlier except that $ZnCl_2$ was omitted from the reaction buffer. Geranylgeranyl diphosphate (30 $\mu$M final concentration) was used, instead of FPP, to show substrate protection. In all cases, enzyme concentrations were determined via the method of Bradford using bovine serum albumin (BSA) as a standard (34).

### Photolabeling of enzymes with [$^{32}$P]DATFP-Dihydroester ([$^{32}$P]4)

Samples of [$^{32}$P]**4** (5 $\mu$M) were photolyzed in 52 mM Tris HCl, pH 7, 5.8 mM DTT, 12 mM $MgCl_2$, 12 mM $ZnCl_2$, and 25 $\mu$M FPP dissolved in either 25 mM $NH_4HCO_3$ or the equivalent volume of 25 mM $NH_4HCO_3$ (where appropriate) in a final volume of 100 $\mu$L. In experiments employing purified enzymes (ScPFTase, EcFPPSase and NoS-TSase), the final concentrations of the proteins were 0.05 mg/mL; for experiments with crude *E. coli* lysate containing ScPFTase, a final protein concentration of 0.81 mg/mL was employed. Enzyme concentrations were determined via the method of Bradford using BSA as a standard (34). Samples were irradiated for 5 min using the apparatus described earlier. After photolysis, 50 $\mu$L of loading buffer (see the previous text) was added to each sample before heating to 60 °C for 20 min. Analysis was accomplished via electrophoresis using a 12% Tris-glycine SDS–PAGE gel and subsequent staining with Sypro Orange followed by phosphor imaging to visualize the radiolabeled bands.

### Docking of 4 in the active sites of R. norvegicus protein farnesyltransferase (RnPFTase)

For modeling compound **4** in the active site of RnPFTase (pdb file 1JCR) (35), docking was performed using Glide (Schrodinger, version 5.5). A standard precision docking parameter was set, and 10 000 ligand poses per docking were run. Five resulting conformations with the lowest docking score for each enantiomer (*R*-**4** and *S*-**4**) were chosen. Each one of those was then subjected to quantum mechanics molecular mechanics (QM-MM) using QSITE (Schrodinger, (New York, NY) version 5.5). The three conformations with the overall lowest energy were chosen for display for each enantiomer.

### X-Ray crystallography studies of RnPFTase

Crystals of the RnPFTase:**4** complexes were prepared by soaking **4** into preformed crystals using methods previously described (36). X-ray diffraction data for the PFTase:**4** complex was collected on a Rigaku FRE rotating anode generator equipped with VariMax HR optics and a Raxis-IV++ image plate detector. The detector set at 150 mm, data were collected in 200 contiguous 0.30° oscillation images each exposed for 5 min. The data extend to 2.05 Å resolution and have a $R_{merge}$ of 6.1% with a 3.8-fold multiplicity. The structure was refined using autoBUSTER Global Phasing Limited (Cambridge, UK) to an $R_{factor}$ of 18.1% and an $R_{free}$ of 21.5%. The coordinates for the structure have been deposited in the Protein Data Bank (3KSL).

### Electrostatic potential calculations of 1 and 4

Structures of **1** and **4** were generated in Gaussian View, and the geometries were optimized at the b3lyp/6-31G(d) level using Gaussian 03 (M.J. Frisch, G.W. Trucks, H.B. Schlegel *et al.*, Gaussian 03, Revision E.01, Gaussian, Inc., Wallingford, CT, 2004). The extended conformation of each molecule was produced by constraining the distance between remote atoms. A map of electrostatic potential and a map of the electron density were generated for each molecule. To generate the molecular electrostatic potential (MEP), the electrostatic potential was plotted on an isodensity surface (Molecular orbital (MO) = 0.02 and density = 0.02) using Gaussian view. The minimum and maximum potentials were set to −0.05 and 0.2, respectively. Calculations of total polar surface area and LogP were performed using ChemBioDraw Ultra (v. 11.0.1) CambridgeSoft (Cambridge, MA).

## Results and Discussion

### *Synthesis of DATFP-amide 3*

The amide-containing analog **3** was prepared using the route shown in Scheme 1. Amine **6** was prepared as previously described

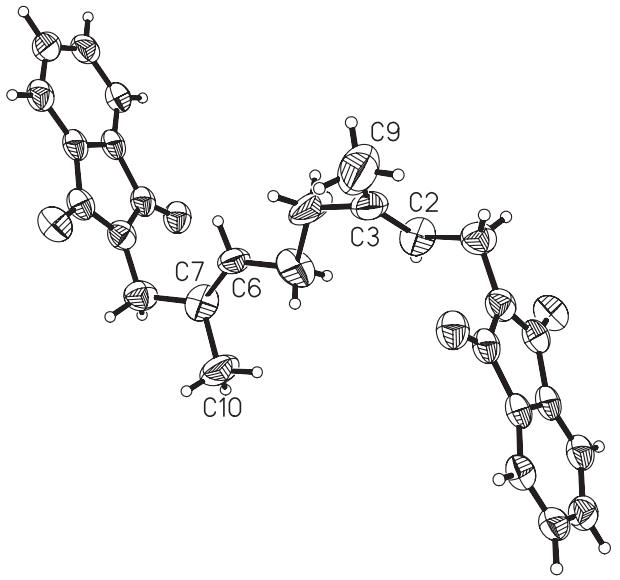


**Figure 2:** Structure of compound **10** determined by X-ray crystallography to establish the *E* stereochemistry of the C-6 alkene.

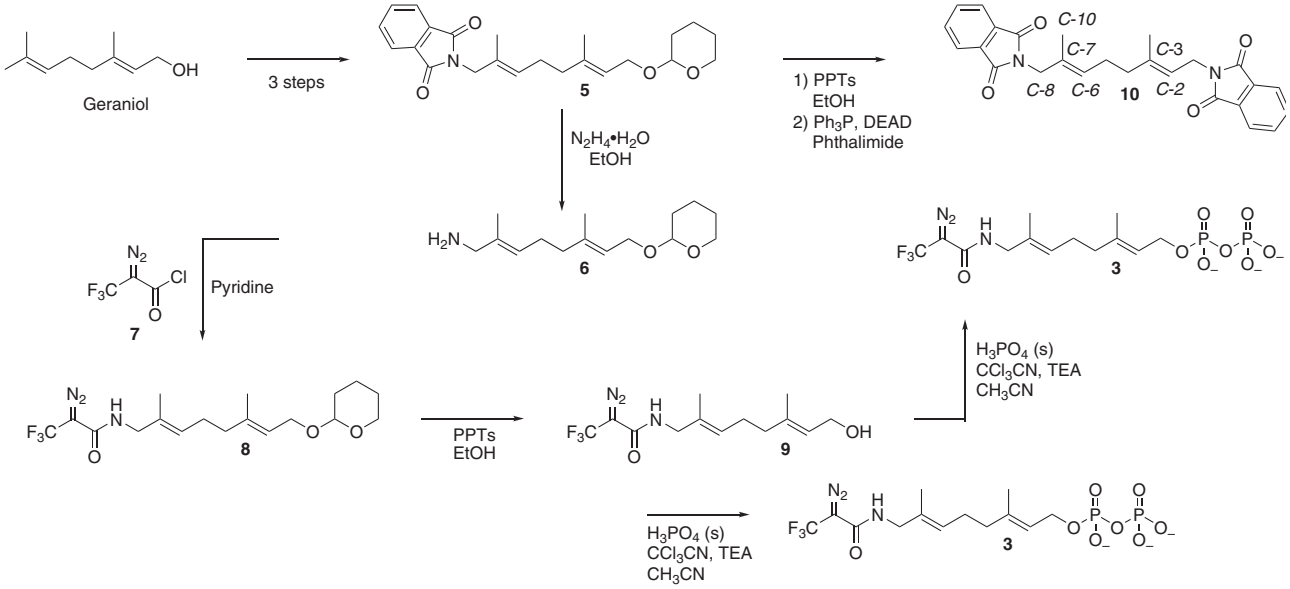


**Scheme 1:** Synthesis of amide-linked photoaffinity analog **3**.

**Figure 3:** Rearrangement of diazotrifluoropropanoyl-amides to triazolones.

(19) and acylated with DATFP-Cl (30) (**7**) in pyridine to produce the protected intermediate **8**. That compound was subsequently deprotected and phosphorylated using the method of Cramer (37,38) to yield a mixture mono and diphosphates. Pure diphosphate **3** was obtained by reversed-phase HPLC and characterized by $^{1}$H-NMR, MS, and UV/vis spectrophotometry. While the regioselectivity of geraniol hydroxylation with $SeO_2$ has been established in other cases (39), we elected to confirm this in the Tetrahydropyran (THP)-protected version by converting intermediate **5** to the corresponding bis-phthalimide derivative **10**. That transformation was accomplished by THP removal followed by subsequent Mitsunobu reaction (40,41) to yield **10** whose structure was then confirmed via x-ray crystallography. The *E* stereochemistry of the 6,7 alkene is apparent in the structure of this derivative shown in Figure 2. For photolabeling experiments, radiolabeled **3** was prepared via phosphorylation of alcohol **9** with [$^{32}$P]-$H_3PO_4$ as previously described (42). Solutions of **3** in aqueous $NH_4HCO_3$ are stable for several weeks when stored at 4 °C. However, storage for longer periods of time results in a change in the UV spectrum from $\lambda_{max}$ = 238 nm to $\lambda_{max}$ = 250 nm with no change in the mass spectrum of the compound; these observations are indicative of isomerization of the diazo amide to the corresponding triazolone (see Figure 3) (43,44). Thus, for maximal crosslinking efficiency compound **3** must be used within one month of its synthesis.

### *Enzymatic studies with PFTase using DATFP-amide 3*

Initially, a continuous fluorescence assay was used to determine whether or not the new photoaffinity analog **3** is a substrate for

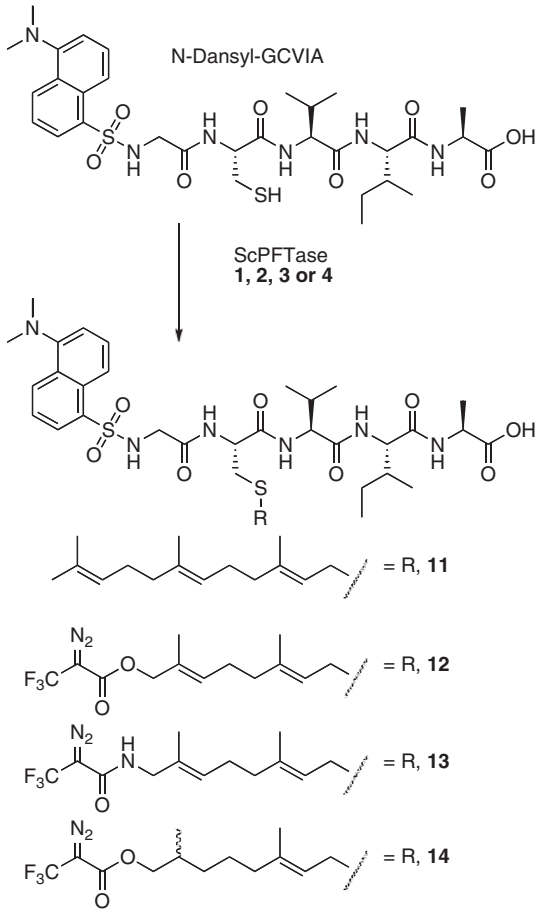


**Scheme 2:** Structures of *Saccharomyces cerevisiae* protein farnesyltransferase modified *N*-dansyl-GCVIA peptide products. **11**: peptide product from reaction with farnesyl diphosphate (**1**); **12**: peptide product from reaction with allylic ester **2**; **13**: peptide product from reaction with amide **3**; **14**: peptide product from reaction with alkyl ester **4**.

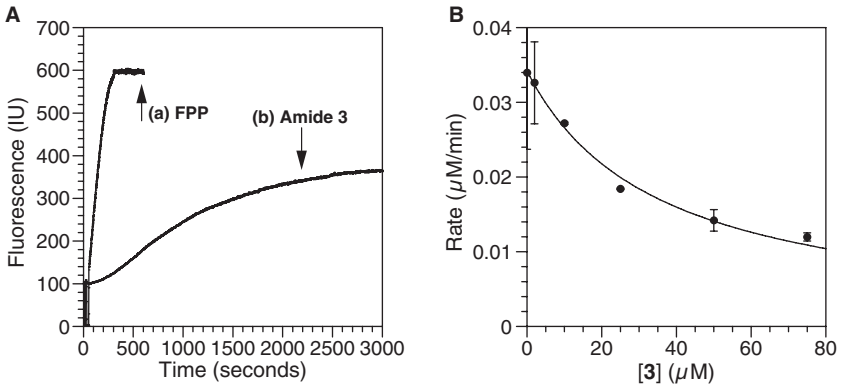


**Figure 4:** Evaluation of amide **3** as an alternative substrate and inhibitor of *Saccharomyces cerevisiae* protein farnesyltransferase (ScPFTase). (A) Reaction between *N*-dansyl-GCVIA and farnesyl diphosphate (FPP) or amide **3** catalyzed by ScPFTase monitored by fluorescence spectroscopy. (a) Kinetic data using FPP as a substrate. (b) Kinetic data using amide **3** as a substrate. Fluorescence was monitored at 30 °C by excitation at 340 nm and emission at 505 nm. (B). Inhibition of ScPFTase-catalyzed farnesylation of *N*-dansyl-GCVIA by amide **3**. Reactions contained 2.0 μM FPP, 2.0 μM *N*-dansyl-GCVIA, and **3** at varying concentrations and were monitored using a continuous spectrofluorometric assay. Each point is the average of 2–3 determinations with the error bars indicating the standard error for each measurement.

ScPFTase. Incubation of the substrate peptide *N*-dansyl-GCVIA with FPP resulted in a rapid increase in dansyl group fluorescence (see Figure 4A, trace a) because of the production of the farnesylated product **11** (see Scheme 2). Replacing the natural substrate, FPP, with 10 $\mu$M amide **3** in the assay resulted in a similar time-dependent increase in fluorescence, suggesting that the analog is a substrate for the enzyme (see Figure 4A, trace b); interestingly, the fluorescence plateaued at a lower value than that obtained with FPP suggesting that the prenylated product **13** is less fluorescent than **11**. However, importantly, the fluorescence increased at a much slower rate with 10 $\mu$M **3** than with 10 $\mu$M FPP and much longer reaction times (3000 seconds) were required for significant conversion to product compared with 200 seconds for complete conversion to the farnesylated peptide product. Also, a significantly higher concentration of enzyme (92 nM) was used, compared with 2.5 nM normally added for assays with FPP as the substrate. Based on those numbers, we estimate that **3** functions some 250-fold times slower than FPP as a substrate for ScPFTase. To verify that **3** is a substrate for the enzyme, the product from a large-scale enzyme reaction (15 mL) was purified by reversed-phase HPLC and analyzed by MS. The fast atom bombardment mass spectrometry (FAB-MS) spectrum showed a $[M+H]^+$ peak of 982.5 and a $[M+Na]^+$ peak at 1004.6, corresponding to the expected peptide product (**13**).

Because DATFP-amide **3** appeared to be a significantly slower substrate than FPP for ScPFTase, the analog was evaluated as an inhibitor of the reaction between FPP and the peptide substrate *N*-dansyl-GCVIA. An $IC_{50}$ value of 50 $\mu$M (see Figure 4B) was obtained for the inhibition of ScPFTase by **3** that is significantly higher than the value of 0.72 $\mu$M measured for the corresponding ester-linked compound **2** (5). This higher value suggests lower affinity for the amide-containing analog and may reflect the more rigid nature of the amide-linked analog versus ester-linked analog.

### *Photolysis experiments with DATFP-amide 3*

Amide **3** was first evaluated for its ability to label ScPFTase. UV irradiation of ScPFTase in the presence of 15 $\mu$M [$^{32}$P]**3** at 254 nm for 1 min resulted in preferential labeling of the 43 kDa $\beta$ subunit (Figure 5, Lane 3′); inclusion of 30 $\mu$M FPP in the reaction mixture gave substantial protection from labeling (Lane 4′, 3% of the crosslinking observed in Lane 3′). This selective labeling of the $\beta$-subunit is consistent with previous results with DATFP esters and suggests that the isoprenoid moiety interacts predominantly with the $\beta$-subunit when it binds to the enzymatically active $\alpha,\beta$-heterodimer. Similar results were obtained with HsPGGTase I where UV irradiation of purified enzyme in the presence of 15 $\mu$M [$^{32}$P]DATFP-GPP amide at 254 nm for 1 min resulted in preferential labeling of the 43 kDa $\beta$ subunit (Figure 6, Lane 2′); inclusion of 30 $\mu$M geranylgeranyl diphosphate (GGPP) in the reaction mixture resulted in substantial protection from labeling (Lane 3′, 5% of the crosslinking observed in Lane 2′). It is interesting to note that a small amount of labeling of the $\alpha$-subunit was also observed with this enzyme. This may reflect an alternative binding mode for the probe; crystallographic studies suggest that a second isoprenoid binding site exists in PGGTase that is involved in interactions with the prenylated product (45). Finally, we explored the photolysis of *Rattus norvegicus* protein geranylgeranyltransferase type II (RnPGGTase II) in the presence of **3** because there have been no reported studies of photoaffinity labeling of the type II enzyme with DATFP-based probes. UV irradiation of RnPGGTase II in the presence of 10 $\mu$M [$^{32}$P]**3** resulted in preferential labeling of the 38 kDa $\beta$ subunit (Figure 7, Lane 2′). As was observed in the cases noted earlier including 30 $\mu$M GGPP in the reaction mixtures gave substantial protection from labeling (Lane 3′, 9% of the crosslinking observed in Lane 2′). These results give direct evidence for the involvement of the $\beta$ subunit of

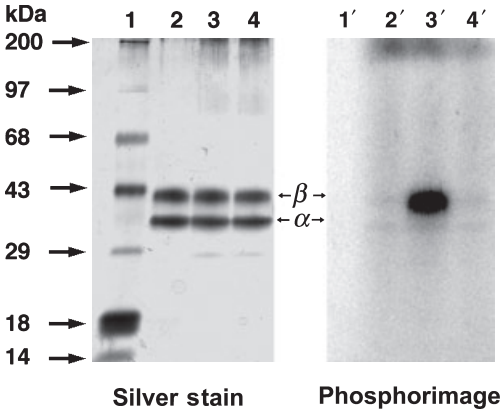


**Figure 5:** Analysis of photolabeling of *Saccharomyces cerevisiae* protein farnesyltransferase with diazotrifluoropropanoyl-amide ([$^{32}$P]**3**) by SDS–PAGE. Lanes 1 and 1′: molecular weight standards. Lanes 2 and 2′: sample containing protein farnesyl transferase (PFTase) and [$^{32}$P]**3**, no UV irradiation. Lanes 3 and 3′: PFTase irradiated in the presence of [$^{32}$P]**3**. Lanes 4 and 4′: PFTase irradiated in the presence of [$^{32}$P]**3** and farnesyl diphosphate (substrate). Lanes 1, 2, 3, and 4 show the silver-stained proteins. Lanes 1′, 2′, 3′, and 4′ show the radiolabeled proteins.

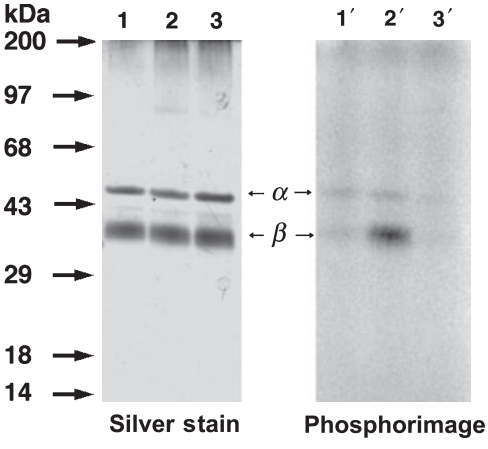


**Figure 6:** Analysis of photolabeling of *H. sapiens* protein geranylgeranyltransferase type 1 (HsPGGTase I) with diazotrifluoropropanoyl-amide ([$^{32}$P]**3**) by SDS–PAGE. Lanes 1 and 1′ contain samples of PGGTase I and [$^{32}$P]**3** that were not irradiated. Lanes 2 and 2′ contain samples of HsPGGTase I irradiated at 254 nm in the presence of [$^{32}$P]**3**. Lanes 3 and 3′ contain samples of PGGTase I irradiated in the presence of [[$^{32}$P]**3** and farnesyl diphosphate (substrate). Lanes 1, 2, and 3 show the silver-stained proteins. Lanes 1′, 2′, and 3′ show the radiolabeled proteins.

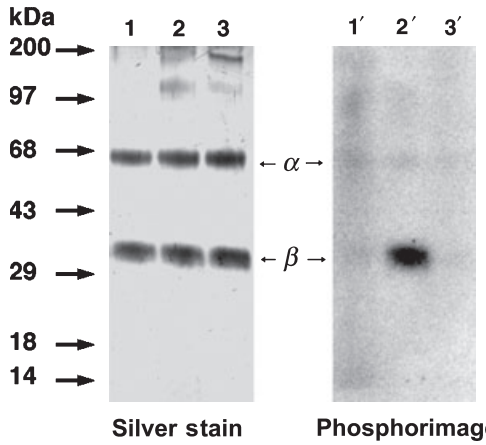


**Figure 7:** Analysis of photolabeling of *R. norvegicus* protein geranylgeranyltransferase type 2 (RnPGGTase II) with diazotrifluoropropanoyl-amide ([$^{32}$P]**3**) by SDS–PAGE. Lanes 1 and 1′: PGGTase II and [$^{32}$P]**3**, no UV irradiation. Lanes 2 and 2′: RnGGPTase II and [$^{32}$P]**3**, 1 min UV irradiation. Lanes 3 and 3′: RnPGGTase II, [$^{32}$P]**3**, and geranylgeranyl diphosphate, 1 min UV irradiation. Lanes 1, 2, and 3 show the silver-stained proteins. Lanes 1′, 2′, and 3′ show the radiolabeled proteins.

RnGGPTase II in isoprenoid substrate binding that is consistent with crystallographic data on this system (46,47). Also, because these experiments were carried out in the absence of the escort protein, REP-1, the results indicate that this protein is not necessary for isoprenoid substrate binding.

### *Synthesis of dihydroester 4*

While the amide linkage present in **3** did contribute to its enhanced stability, the rearrangement of the diazo amide to the triazolone shown in Figure 3 limited the utility of this compound. Thus, we undertook the synthesis of dihydroester-linked analog **4** that was prepared using the route shown in Scheme 3. THP protection of geraniol followed by allylic oxidation and selective reduction of the $\alpha,\beta$-unsaturated aldehyde afforded **15** as previously described (26). That alcohol was acylated with DATFP-Cl (**7**), deprotected and phosphorylated using the method of Cramer (38). For photolabeling experiments, radiolabeled **4** was prepared via phosphorylation of alcohol **17** with [$^{32}$P]$H_3PO_4$ using a procedure previously described for related analogs (31). It should be noted that **4** contains a stereogeneic center (C-7) and is hence chiral. No attempt was made to resolve the enantiomers, and thus all experiments were performed with racemic material.

### *Stability studies of alkyl and allylic DATFP esters*

To investigate the stability of the dihydro isoprene unit in **4** compared with its allylic counterpart present in **2**, five carbon DATFP-containing model compounds were synthesized. Compound **18** (Scheme 4) contains a DATFP moiety linked to an allylic alcohol to model compound **2** while **19** lacks the allylic alcohol and is hence designed to mimic **4**. Model compounds **18** and **19** were synthesized by reaction of DATFP-Cl (**7**) with dimethylallyl alcohol or isopentenyl alcohol, respectively.

As a test of stability, compounds **18** and **19** were treated with a solvent mixture consisting of $CD_3CN/D_2O$ (9/1, v/v) containing 0.1% TFA-*d*. That mixture was used here because it is representative of what is typically employed for peptide extraction from gels and subsequent chromatographic fractionation. Deuterated solvents were used to allow direct analysis of the reaction mixtures to be performed by $^1$H-NMR. Portions of the spectral data from **18** and **19** prior to reaction are shown Figure 8 (panels A and C, respectively). Treatment of allylic ester **18** in the solvent mixture described earlier at 100 °C for 4 h resulted in substantial hydrolysis to produce primarily tertiary alcohol **21** together with traces of several other products including allylic alcohol **20** as evidenced from the H-NMR.

NMR spectrum (Figure 8B) of the reaction mixture; in addition to unreacted starting material, the observation of three doublet of

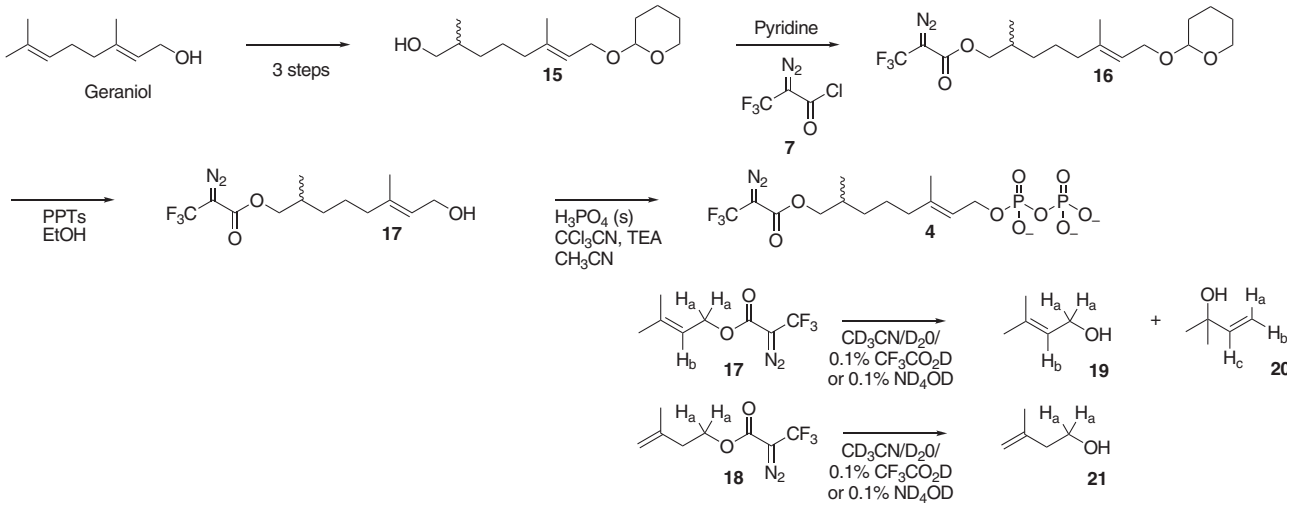


**Scheme 3:** Synthesis of dihydroester-linked photoaffinity analog **4**.

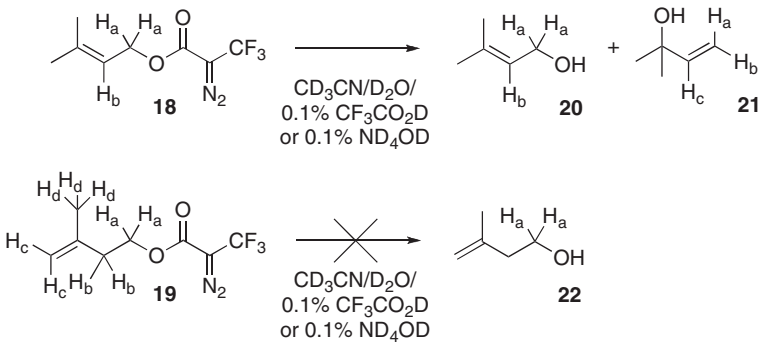


**Scheme 4:** Diazotrifluoropropanoyl-containing allylic ester and alkyl ester model compounds and their putitive hydrolysis products.

doublets at 4.92, 5.13, and 5.96 ppm confirms the presence of **21**. In contrast, incubation of the homoallylic ester **19** under identical conditions resulted in no changes in the $^1$H NMR spectrum (Figure 8D) of the corresponding reaction mixture (compare Figure 8C with Figure 8D); no evidence for the formation of **22** was observed. These results indicate that **19** is substantially more stable than **18** under these mildly acidic conditions and suggest that crosslinked products derived from reactions with probe **4** (homoallylic ester) should be significantly more resistant to hydrolytic degradation than products obtained with allylic ester **2**.

### *Enzymatic studies with PFTase using dihydroester 4*

To evaluate dihydroester **4** as a substrate, we initially utilized the continuous fluorescence assay employed to study amide **3**. Those

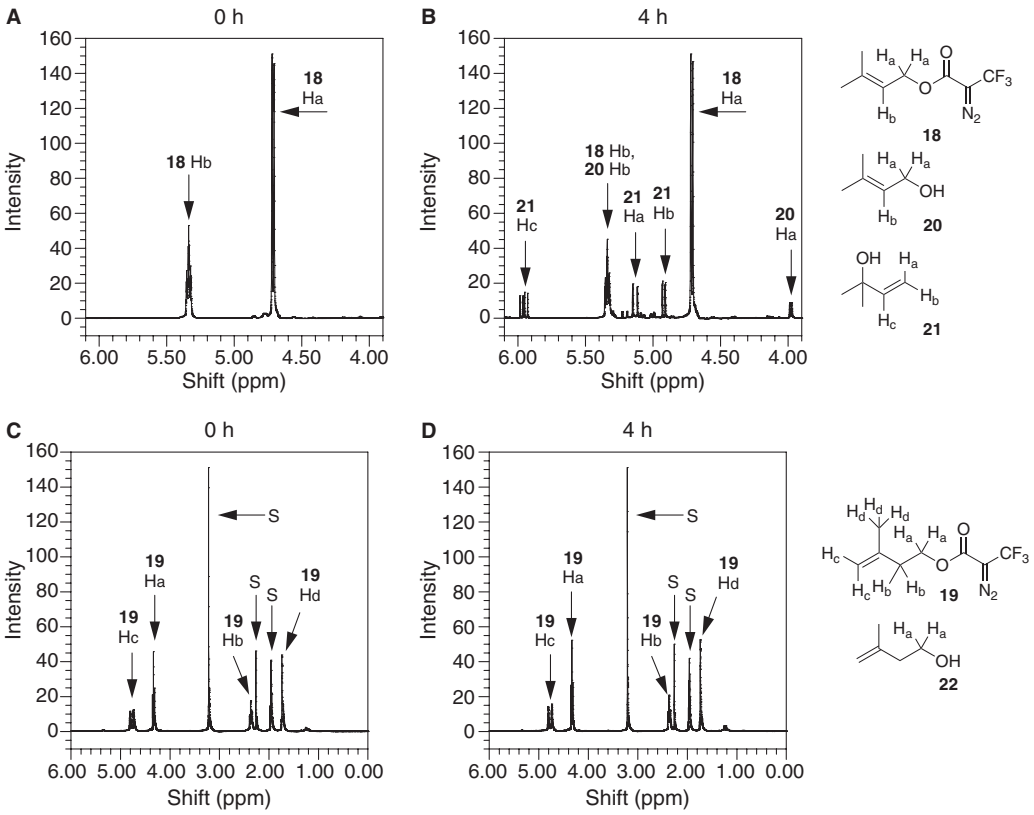


**Figure 8:** $^1$H-NMR spectra of diazotrifluoropropanoyl-containing model esters obtained under mild acidolytic conditions. Spectra on the left are the compounds before heating, and spectra on the right are the compounds after heating at 100 °C for 4 h. (A) Compound **18** treated under acidic conditions ($CD_3CN/D_2O$ 10%/trifluoroacetic acid (TFA)-*d* 0.1%) before heating. (B) Compound **18** treated under acidic conditions ($CD_3CN/D_2O$ 10%/TFA-*d* 0.1%) after heating to 100 °C for 4 h. The appearance of three new doublets of doublets after heating indicates the presence of **21**. (C) Compound **19** treated under acidic conditions ($CD_3CN/D_2O$ 10%/TFA-*d* 0.1%) before heating. (D) Compound **19** treated under acidic conditions ($CD_3CN/D_2O$ 10%/TFA-*d* 0.1%) after heating to 100 °C for 4 h. Compound **19** shows no visible change in the $^1$H-NMR spectrum after 4 h. In panels (C) and (D), peaks labeled 'S' are from $D_2O$, *p*-xylene (internal standard for integration), and $CD_3CN$.

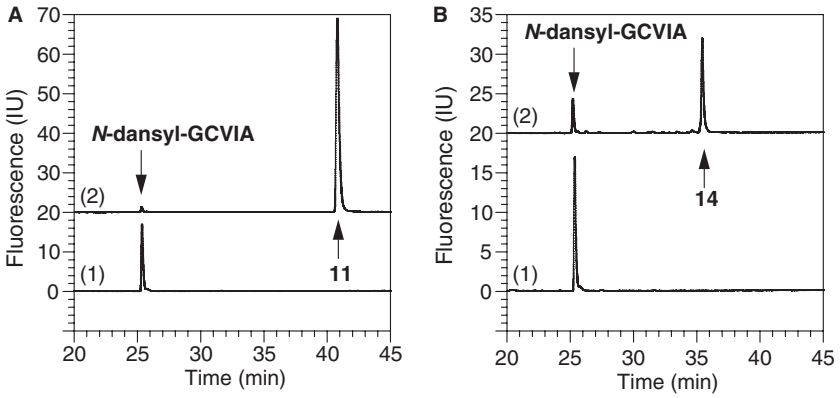


**Figure 9:** Reversed-phase HPLC analysis with fluorescence detection of reactions between *N*-dansyl-GCVIA and farnesyl diphosphate (FPP) (**1**) or dihydroester **4** catalyzed by *Saccharomyces cerevisiae* protein farnesyltransferase (ScPFTase). (A) *N*-dansyl-GCVIA (2.4 $\mu$M) incubated with FPP (**1**, 10 $\mu$M) and ScPFTase (24 nM). Chromatogram 1 (bottom): Reaction before the addition of the enzyme with the peptide eluting at $t_R$ = 25.7 min. Chromatogram 2 (top): Reaction after 5 min with the prenylated peptide (**11**) appearing at $t_R$ = 41.5 min. (B) *N*-dansyl-GCVIA (2.4 $\mu$M) incubated with dihydroester (**4**, 10 $\mu$M) and ScPFTase (24 nM). Chromatogram 1 (bottom): Reaction before the addition of the enzyme with the peptide substrate at $t_R$ = 25.7 min. Chromatogram 2 (top): Reaction after 23 h with the prenylated peptide (**14**) appearing at $t_R$ = 36.0 min and some starting material still present.

experiments gave similar results as were observed with **3**, suggesting that compound **4** was a slow alternative substrate for ScPFTase. However, unambiguous interpretation of the data was made difficult because of slow, time-dependent perturbations of the fluorescence of the putative prenylated peptide product (**14**, see Scheme 2). It has been previously noted that the fluorescence assay is sensitive to small changes in the reaction conditions (32,33) and that some isoprenoid analogs that are alternative substrates modulate the fluorescence of the starting peptide and product (48,49). Hence, we elected to monitor the enzymatic reactions by a method that is less prone to such artifacts. Accordingly, the incorporation of **4** into a peptide substrate was monitored by reversed-phase HPLC using fluorescence detection. When the natural substrate FPP (10 $\mu$M) was incubated with *N*-dansyl-GCVIA (2.4 $\mu$M) and ScPFTase (24 nM), near complete conversion (93%) to the prenylated peptide product (**11**) was observed within 5 min (Figure 9A). The reaction of **4** (10 $\mu$M) with *N*-dansyl-GCVIA (2.4 $\mu$M) and ScPFTase (24 nM) to yield **14**, however, was still not complete after 23 h (Figure 9B). Based on peak integrations, prenylation of the dansylated peptide with the unnatural substrate **4** was 77% complete after 23 h, making it approximately 300 times slower than the same reaction with FPP. The lower rate observed with **4** is comparable to that observed with **2** and **3** (see the previous text). However, it should be noted that if extensive conversion is desired, the lower efficiency of incorporation manifested by these compounds can generally be compensated for by the employment of higher enzyme concentrations and longer reaction times. Moreover, methods have been developed for the purification of both prenylated peptides (conventional reversed-phase HPLC) and proteins (cyclodextrin affinity chromatography) (50). Thus, this lower efficiency of incorporation does not represent a serious limitation for applications with these analogs even if the goal is to produce proteins or peptides that incorporate these photoactive isoprenoids.

Because dihydroester **4** appeared to be a significantly slower substrate than FPP for ScPFTase, the analog was evaluated as an inhibitor of the reaction between FPP and the peptide substrate *N*-dansyl-GCVIA. An $IC_{50}$ value of 30 $\mu$M (see Figure 10) was obtained for the inhibition of ScPFTase by **4.** That value is 1.7-fold lower than that for **3** but still significantly higher than that observed for **2** (0.7 $\mu$M) (5); these data show how sensitive the enzyme is to even small perturbations in the isoprenoid structure. This result is perhaps not surprising because both the first and the second isoprenoid units from FPP undergo conformational changes as the enzyme proceeds from the ternary complex to the product complex (51).

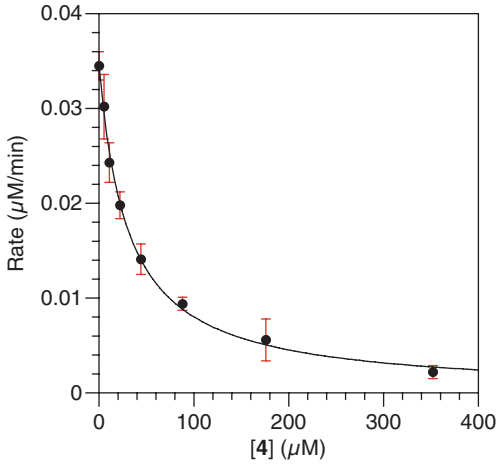


**Figure 10:** Inhibition of *Saccharomyces cerevisiae* protein farnesyltransferase-catalyzed farnesylation of *N*-dansyl-GCVIA by dihydroester **4**. Reactions contained 2.0 $\mu$M farnesyl diphosphate, 2.0 $\mu$M *N*-dansyl-GCVIA, and **4** at varying concentrations and were monitored using a continuous spectrofluorometric assay. Each point is the average of three determinations with the error bars indicating the standard error for each measurement.

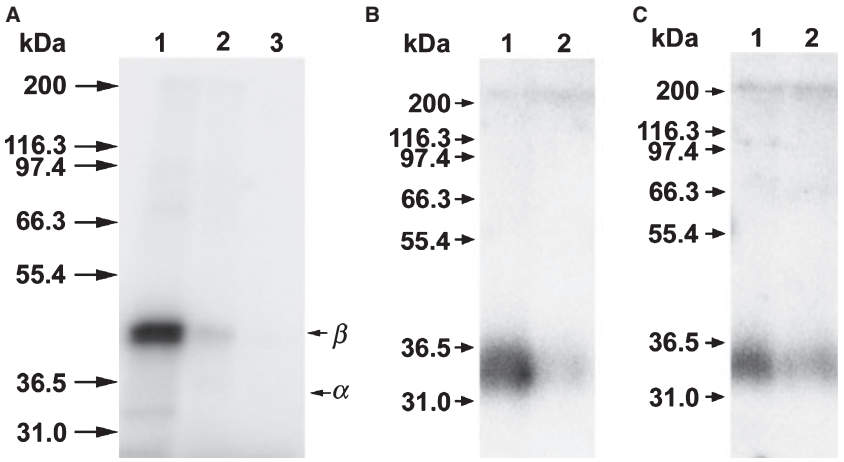


**Figure 11:** Analysis of photolabeling of purified farnesyl diphosphate (FPP)-utilizing enzymes with dihydroester [$^{32}$P]**4**. For all samples, photolysis reactions were fractionated by SDS–PAGE followed by phosphor imaging analysis to allow visualization of the radiolabeled proteins. In each case, Lane 1 contains enzyme irradiated in the presence of [$^{32}$P]**4** while Lane 2 contains enzyme irradiated in the presence of [$^{32}$P]**4** and FPP (substrate). Where shown, Lane 3 contains [$^{32}$P]**4** incubated in the presence of protein without irradiation. Panel A: Analysis of photolabeling of purified protein farnesyl transferase. Panel B: Analysis of photolabeling of purified *E. coli* farnesyl diphosphate synthase. Panel C: Analysis of photolabeling of purified *Nostoc sp. strain PCC7120* sesquiterpene synthase.

### *Photolysis experiments with dihydroester 4*

To compare the properties of dihydroester **4** and amide **3**, compound **4** was evaluated for its ability to label ScPFTase. UV irradiation of ScPFTase in the presence of 15 $\mu$M [$^{32}$P]**4** at 254 nm for 1 min resulted in preferential labeling of the 43 kDa $\beta$ subunit (see Figure 11A, Lane 1). Inclusion of 30 $\mu$M FPP in the reaction mixture gave substantial protection from labeling, reducing the amount of crosslinking to 20% of that obtained in the absence of FPP (Lane 2); no labeling was observed in unphotolyzed reaction mixtures (Lane 3). This selective labeling of the $\beta$-subunit is similar to what is observed in experiments with **2** and **3**. We next wanted to explore the ability of **4** to label other FPP-utilizing enzymes to gain insight into the scope of this probe. Thus, *E. coli* farnesyldiphosphate synthase (EcFPPSase) was irradiated in the presence of [$^{32}$P]**4**, and the reaction analyzed in a manner analogous to that employed above with ScPFTase. The results of this experiment are shown in Figure 11B; Lane 1 shows significant labeling of the protein while Lane 2 shows a decrease in labeling (29% of the labeling observed in Lane 1) when the photolysis was performed in the presence of both [$^{32}$P]**4** and FPP as a competitor. Similar results were obtained in labeling experiments with a germacrene-producing, sesquiterpene synthase from a cyanobacterial source, *Nostoc sp. strain PCC7120* (NoSTSase). Lane 1 (Figure 11C) illustrates the labeling of the enzyme by [$^{32}$P]**4** while Lane 2 shows the results when the photolysis was performed in the presence of both [$^{32}$P]**4** and FPP; a significant (although not as great as for the other enzymes studied) decrease in labeling (58% of the labeling observed in Lane 1) was again observed when the reaction was carried out in the presence of the competitor (FPP). Finally, to evaluate the specificity of [$^{32}$P]**4**, photolabeling was performed on a complex mixture of proteins containing ScPFTase present at low concentration. We routinely purify ScPFTase by expressing the genes in *E. coli*; based on activity assays, we estimate that ScPFTase is present in crude soluble extract as 1% of the total protein.

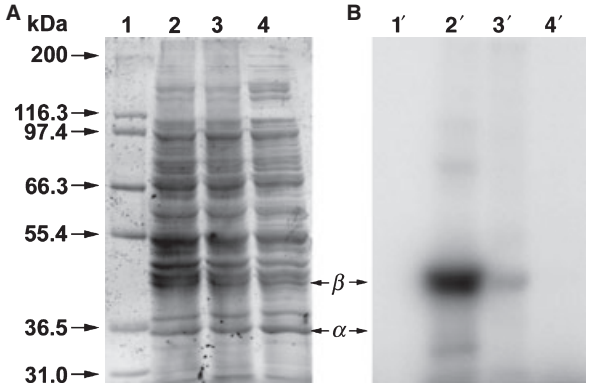


**Figure 12:** Selective photolabeling of ScyPFTase in crude *E. coli* extract using dihydroester **4**. Analysis of photolabeling of *Saccharomyces cerevisiae* protein farnesyltransferase (ScPFTase) with [$^{32}$P]**4** by SDS–PAGE. Lanes 1 and 1′: Molecular weight standards. Lanes 2 and 2′: Crude ScPFTase irradiated in the presence of [$^{32}$P]**4**. Lanes 3 and 3′: Crude ScPFTase irradiated in the presence of [$^{32}$P]**4** and farnesyl diphosphate (substrate). Lanes 4 and 4′: Sample containing crude yPFTase and [$^{32}$P]**4**, no UV irradiation. Panel A: Sypro Orange-stained proteins. Panel B: Radiolabeled proteins visualized via phosphor imaging analysis.

Hence, we considered this protein mixture to be a useful benchmark for examining the specificity of these probes. Accordingly, crude *E. coli* extract containing ScPFTase was photolyzed in the presence of 5.0 $\mu$M [$^{32}$P]**4**; results of those experiments are shown in Figure 12. Lane 2 shows the large number of different proteins present in *E. coli* crude extract while lane 2′ reveals only one major photocrosslinked product corresponding to the ScPFTase $\beta$-subunit and a few additional faint bands. As was noted earlier with photolysis reactions employing purified ScPFTase, inclusion of FPP in the

photolysis mixture results in almost complete elimination of photolabeling (Lane 3′). Thus, it appears that [$^{32}$P]**4** can selectively label ScPFTase selectively even in the presence of a large number of other proteins.

### *Docking analysis of dihydroester 4 with RnPFTase*

As noted earlier, excellent selectivity of labeling was obtained with dihydroester **4**. However, it is clear that **4** binds to ScPFTase with significantly less affinity than does FPP; a rough estimation of this difference can be obtained from a comparison of the $IC_{50}$ of **4** reported here for ScPFTase ($IC_{50}$ = 30 $\mu$M) versus the $K_D$ of FPP for PFTase ($K_D$ = 75 nM) (52). To gain insight into why **4** might bind to ScPFTase with attenuated affinity, docking experiments were performed in which the two enantiomers of dihydroester **4** were docked into the structure of RnPFTase. For each enantiomer, an ensemble of poses was obtained; inspection of those structures indicated that the diazoester moiety was twisted significantly from a planar conformation. Consequently, the top five poses for each enantiomer were further optimized by QM-MM calculations. Interestingly, the rank order (based on energy) of the structures obtained following QM-MM energy minimization was different than the order obtained directly from the docking (based on docking scores). In all subsequent discussion, the term 'docked' poses refers to docked poses following QM-MM energy minimization. In general, there was greater variation in the docked *R*-poses (Figure 13A) compared to the docked *S*-poses (Figure 13B) with the greatest variation occurring in the position of the DATFP group. The best structures for each of the two enantiomers preserved the 180 ° dihedral angle between the DATFP-carbonyl and azide groups. Significant deviations in the positioning of the diphosphate groups were observed in the docked *R*-poses compared to the docked *S*-poses. Collectively, these docking experiments predict that dihydroester **4** binds to RnPFTase in the FPP binding site in a fashion similar to FPP although the significant variations observed in the docked structures make a specific conformation difficult to assign.

### *Crystallographic analysis of dihydroester 4 bound to RnPFTase*

Because the docking experiments described earlier suggested that compound **4** would bind in the active site of PFTase in a similar manner as FPP, we sought to confirm this by obtaining a structure of the analog bound to RnPFTase; hence, **4** was soaked into crystals of RnPFTase and the structure determined by X-ray crystallography. Comparison of the protein in the structure of the RnPFTase:**4** complex and the RnPFTase:FPP:SCH66336 ternary complex shows a 0.2 Å r.m.s. deviation for 667 of the 716 C-alpha protein atoms, indicating that no significant domain movements have occurred (36,53). The most significant side chain movement close to **4** is Tyr166$\alpha$, which rotates 75° degrees about chi1 resulting in a 5.5Å movement of the tyrosine hydroxyl (Figure 14C). The electron density resulting from the presence of **4** is shown in Figure 14A; because it was not possible to unambiguously determine whether one or both enantiomers were bound, models for both were fit into the density. A superposition of these models with the previously determined structure for bound FPP is presented in Figure 14B along with a view of the enzyme active site showing both the analog, FPP and the protein surface (Right). In general, the analog (**4**) mimics FPP well. The diphosphate group and first isoprenoid units of **4** closely mirror the corresponding positions in FPP although C-1 in the analog is displaced 0.2 Å for the *S*-enantiomer and 0.9 Å for

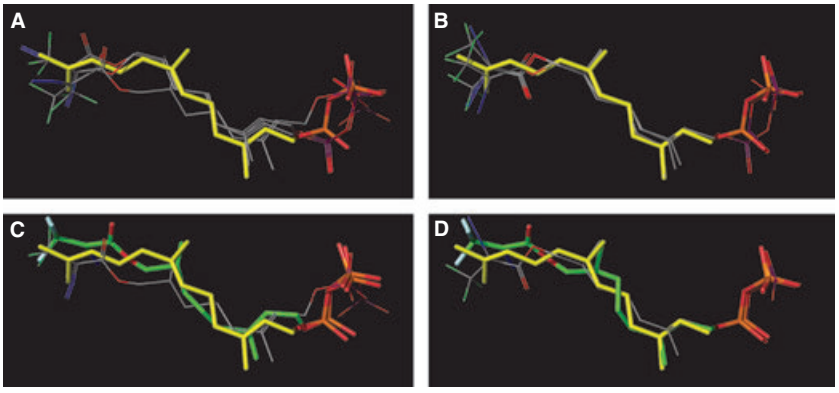


**Figure 13:** Results of docking experiments with dihydroester **4** and RnPFTase. Top Left (A): Top 3 poses for the *R* enantiomer of **4** (line representations) docked into RnPFTase. The position of farnesyl diphosphate (FPP) (stick representation) bound to RnPFTase determined via crystallography (pdb code: 1JCR) is shown for comparison. Top Right (B): Top 3 poses for the *S* enantiomer of **4** docked into RnPFTase. Bottom Left (C): Comparison of highest-scoring docked pose for the *R* enantiomer of **4** (line representation) with the structure of the protein-bound *R* enantiomer determined via crystallography (stick representation, green carbons) and FPP (stick representation, yellow carbons). Bottom Right (D): Comparison of highest-scoring docked pose for the *S* enantiomer of **4** (line representation) with the structure of the protein-bound *S* enantiomer determined via crystallography (stick representation) and FPP (stick representation, yellow carbons). Colors: C (line representations: grey, stick representations: yellow [FPP], green [crystallographic **4**), F (line representations: green, stick representations: white), N (blue), O (red), P (line representations: purple, stick representations: orange). As noted in the text, the term 'docked' pose used here refers to the docked poses that have been subjected to energy minimization.

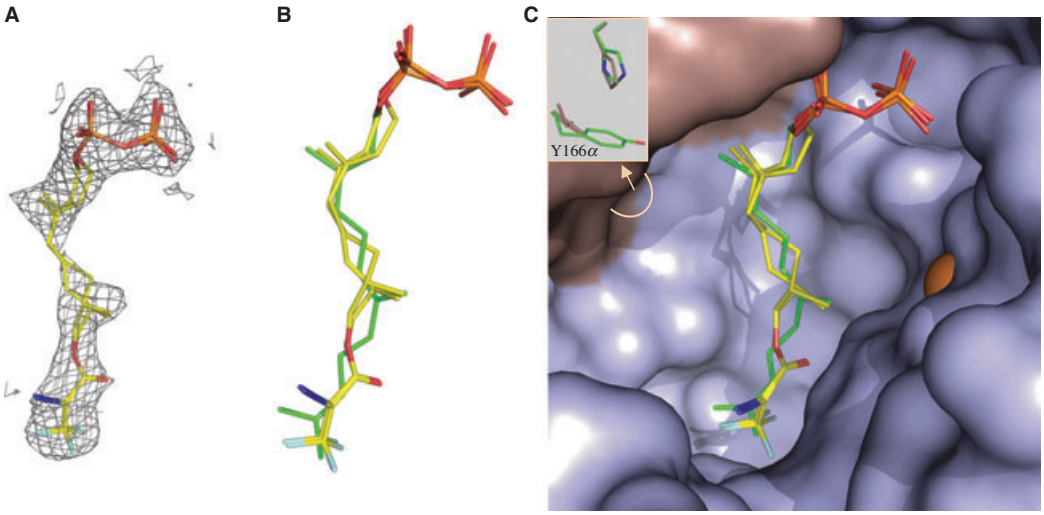


**Figure 14:** Structure of dihydroester **4** bound to RnPFTase determined by X-ray crystallography. (A) Electron density for dihydroester **4** (mesh) contoured at 1.0 $\sigma$. The structures of the two enantiomers of **4** (shown in stick representations) are fit within the electron density. (B) Structures of the two enantiomers of **4** superimposed with the structure of farnesyl diphosphate (FPP) (green) bound to RnPFTase. (C) Active site of RnPFTase showing structures of the two enantiomers of **4** superimposed with the structure of FPP (green). The insert shows the difference in conformation for Y166$\alpha$ and H210$\alpha$ between the structures of **4** and FPP. Colors: C (yellow), N (blue), O (red), $\alpha$-subunit (grey), $\beta$-subunit (light blue), Zn (orange).

the *R*-enantiomer. Additionally, the DATFP group of **4** is positioned similarly to the third isoprenoid unit of FPP although it is also displaced approximately 1.0 Å to one side. The most significant difference lies in the position of the second isoprenoid unit within the analog. Introduction of the sp3 hybridized centers at C-6 and C-7 along with the ester linkage present in the analog results in a significant rotation of the second isoprenoid unit; however, one note of caution that should be acknowledged concerning the structure of the middle isoprenoid element is that the electron density in that region is not well defined (see Figure 14A) making definitive structural assignment difficult. It is interesting to compare the conformation of **4** obtained from crystallography with the best poses obtained from docking. A comparison for the *R*-enantiomer of **4** is shown in Figure 13C and for the *S*-enantiomer in Figure 13D. The best docked pose of *S*-**4** is closer to the conformation of crystallographically determined FPP than to crystallographically determined *S*-**4**; in contrast, the best docked pose of *R*-**4** differs significantly from the crystallographically determined conformations of both FPP and *R*-**4**. These results suggest that while the docking experiments do correctly predict the overall orientation of the bound analog, they are less accurate in predicting the precise conformation of the bound compound. This may reflect that fact that no specific hydrogen bonds or polar interactions occur between the protein and the ligand (except for the diphosphate moiety). Hence, the energetics are dominated by non-directional Van der Waals interactions.

### *Comparison of electrostatic potential calculations of FPP and dihydroester 4*

While the docking calculations described earlier in conjunction with the crystallographic experiments demonstrate that compound **4** can be accommodated into the active site of PFTase, they do not

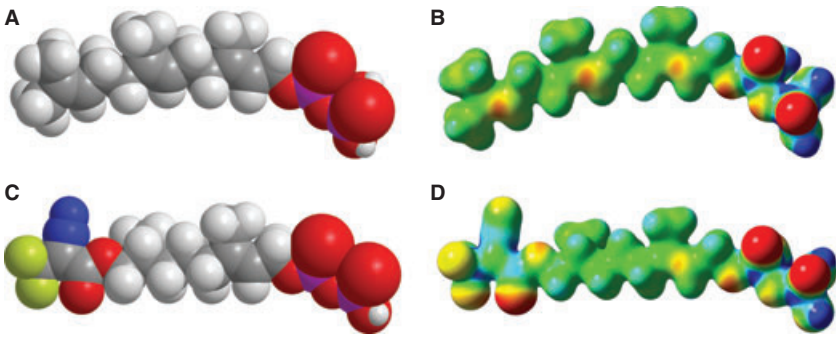


**Figure 15:** CPK models and molecular electrostatic potential (MEP) maps calculated for farnesyl diphosphate (FPP) and dihydroester **4**. Above: CPK model (A) and MEP (B) for FPP. Below: CPK model (C) and MEP (D) for **4**. For MEP maps, potentials were plotted on a surface of constant density (density = 0.02). Electronegative areas are shown in red, and electropositive areas are shown in blue.

explain why the affinity of **4** for the enzyme is so much weaker than that of FPP. To gain insight into that question, Density functional theory (DFT) calculations were employed to calculate the molecular electrostatic potential maps for FPP and **4** presented in Figure 15 (Panels B and D); standard Corey-Pauling-Koltun (CPK) models are also provided in Figure 15 (Panels A and C) and serve to illustrate that the overall size of the DATFP photophore (compare Figure 15A and 15C) is similar to that of the third isoprene unit in FPP. Clearly, based on geometric considerations alone, **4** and FPP are quite similar. However, inspection of the molecular electrostatic potential maps shows how much these molecules differ (compare Figures 15B and 15D). Note the regions of significant negative potential (red and yellow) in the surface of **4** because of the carbonyl oxygen and fluorine atoms. Similarly, significant positive potential is observed because of the presence of the diazo group and the highly polarized $CF_3$-carbon. Overall, **4** exhibits a substantial increase in total polar surface area of 63 $Å^2$. Not surprisingly, this increase in polarity is accompanied by a decrease in the calculated LogP from 5.0 for FPP to 3.9 for **4**. Thus, these calculations suggest that while FPP and **4** are similar in size, the greater polarity of **4** renders its binding within the hydrophobic isoprenoid binding site in PFTase less favorable compared with FPP. However, it should be noted that these calculations, which examine variations in electrostatic potential, may not provide a complete explanation for the behavior of **4**. More subtle factors including the greater flexibility of **4** and the concomitant effect this might have on the entropy of binding may also be operating.

## Conclusions and Future Directions

In an effort to create photoactive analogs of FPP with enhanced stability, two new compounds have been prepared. Probe **3** contains an amide-linked DATFP moiety is an alternative substrate for ScPFTase and covalently modifies a number of prenyltransferases upon photolysis. However, **3** rearranges to a photochemically inactive triazolone limiting its potential utility. Probe **4** employs an alkyl ester in lieu of the allylic ester found in **2**; that substitution renders the linkage between the DATFP group and the isoprenoid significantly more stable to acidic and basic conditions. Compound **4** is an alternative substrate for ScPFTase. Computer assisted docking and crystallographic analysis indicate that **4** binds to RnPFTase in a manner similar (although not identical) to the natural substrate FPP; those suggest that **4** is a reasonable surrogate for a farnesyl group. Photolysis of **4** in the presence of a several different types of FPP-utilizing enzymes results in crosslinking; of particular note, photolysis of **4** in crude *E. coli* extract expressing ScPFTase results in selective labeling of that enzyme even though it is present as approximately 1% of the total protein. We are currently employing **4** in experiments designed to identify proteins involved in latex and sesquiterpene biosynthesis. Finally, the ability to introduce **4** into peptides, established here, suggests that it should be possible to prepare peptides and proteins that incorporate photoactive isoprenoids that can be used to study the processing of prenylated proteins (12,18,54–56). Given our recent development of cell penetrating prenylated peptides, it should be possible to perform these experiments in living cells (57). Efforts to accomplish this are currently under way.

## Acknowledgments

This research was supported by the National Institutes of Health Grants GM58442 (M.D.D.) and GM080299 (C.S.-D.) and by a Fellowship from the Beckman Scholars Program (M. L. H.). This work was carried out in part using computing resources at the University of Minnesota Supercomputing Institute, instrumentation from the University of Minnesota Center for Mass Spectrometry and Proteomics, and facilities of the Masonic Cancer Center.

## References

1. Cane D.E. (1999) Sesquiterpene biosynthesis: cyclization mechanisms. Compr Nat Prod Chem;2:155–200.
2. Davis E.M., Croteau R. (2000) Cyclization enzymes in the biosynthesis of monoterpenes, sesquiterpenes, and diterpenes. Top Curr Chem;209:53–95.
3. Loomis W.D., Croteau R. (1980) Biochemistry of terpenoids. Biochem Plants;4:363–418.
4. Zhang F.L., Casey P.J. (1996) Protein prenylation: molecular mechanisms and functional consequences. Ann Rev Biochem; 65:241–269.
5. Edelstein R.L., Distefano M.D. (1997) Photoaffinity labeling of yeast farnesyl protein transferase and enzymic synthesis of a Ras protein incorporating a photoactive isoprenoid. Biochem Biophys Res Comm;235:377–382.
6. Allen C.M., Baba T. (1985) Photolabile analogs of the allylic pyrophosphate substrate of prenyltransferases. Meth Enzymol; 110:117–124.
7. Baba T., Allen C.M. (1984) Inactivation of undecaprenylpyrophosphate synthetase with a photolabile analogue of farnesyl pyrophosphate. Biochemistry;23:1312–1322.
8. Baba T., Muth J., Allen C.M. (1985) Photoaffinity labeling of undecaprenyl pyrophosphate synthetase with a farnesyl pyrophosphate analogue. J Biol Chem;260:10467–10473.
9. Omer C.A., Kral A.M., Diehl R.E., Prendergast G.C., Powers S., Allen C.M., Gibbs J.B., Kohl N.E. (1993) Characterization of recombinant human farnesyl-protein transferase: cloning, expression, farnesyl diphosphate binding, and functional homology with yeast prenyl-protein transferases. Biochemistry;32:5167–5176.
10. Das N.P., Allen C.M. (1991) Inhibition of farnesyl transferases from malignant and non-malignant cultured human lyphocytes by prenyl substrate analogues. Biochem Biophys Res Comm;181: 729–735.
11. Yokoyama K., McGeady P., Gelb M.H. (1995) Mammalian protein geranylgeranyltransferase-i: substrate specificity, kinetic mechanism, metal requirements, and affinity labeling. Biochemistry;34:1344–1354.
12. Kale T.A., Distefano M.D. (2003) Diazotrifluoropropionamido-containing prenylcysteines: syntheses and applications for studying isoprenoid-protein interactions. Org Lett;5:609–612.
13. Marecak D.M., Horiuchi Y., Arai H., Shimonaga M., Maki Y., Koyama T. *et al.* (1997) Benzylphenoxy analogs of isoprenoid diphosphates as photoactivatable substrates for bacterial prenyltransferases. Bioorg Med Chem Lett;7:1973–1978.

14. Zhang Y.-W., Koyama T., Marecak D.M., Prestwich G.D., Maki Y., Ogura K. (1998) Two subunits of heptaprenyl diphosphate synthase of bacillus subtilis form a catalytically active complex. Biochemistry;37:13411–13420.
15. Tian R., Li L., Tang W., Liu H., Ye M., Zhao Z.K. *et al.* (2008) Chemical proteomic study of isoprenoid chain interactome with a synthetic photoaffinity probe. Proteomics;8: 3094–3104.
16. DeGraw A.J., Zhao Z., Hsieh J., Jefferies M., Distefano M.D., Strickland C.L. *et al.* (2007) A photoactive isoprenoid diphosphate analogue containing a stable phosphonate linkage: synthesis and structural biochemical studies with prenyltransferases. J Org Chem;72:4587–4595.
17. Turek T.C., Gaon I., Distefano M.D., Strickland C.L. (2001) Synthesis of farnesyl diphosphate analogues containing ether-linked photoactive benzophenones and their application in studies of protein prenyltransferases. J Org Chem;66:3253–3264.
18. Kale T.A., Raab C., Yu N., Dean D.C., Distefano M.D. (2001) A photoactivatable prenylated cysteine designed to study isoprenoid recognition. J Am Chem Soc;123:4373–4381.
19. Turek T.C., Gaon I., Gamache D., Distefano M.D. (1997) Synthesis and evaluation of benzophenone-based photoaffinity labeling analogs of prenyl pyrophosphates containing stable amide linkages. Bioorg Med Chem Lett;7:2125–2130.
20. Turek T.C., Gaon I., Distefano M.D. (1996) Analogs of farnesyl pyrophosphate incorporating internal benzoylbenzoate esters: synthesis, inhibition kinetics and photoinactivation of yeast protein farnesyltransferase. Tet Lett;37:4845–4848.
21. Gaon I., Turek T.C., Weller V.A., Edelstein R.L., Singh S.K., Distefano M.D. (1996) Photoactive analogs of farnesyl pyrophosphate containing benzoylbenzoate esters: synthesis and application to photoaffinity labeling of yeast farnesyltransferase. J Org Chem;61:7738–7745.
22. Gaon I., Turek T.C., Distefano M.D. (1996) Farnesyl and geranylgeranyl pyrophosphate analogs incorporating benzoylbenzyl ethers: synthesis and inhibition of yeast protein farnesyltransferase. Tet Lett;37:8833–8836.
23. Rilling H.C. (1985) Photoaffinity substrate analogs for eukaryotic prenyltransferase. Meth Enzymol;110:125–131.
24. Chehade K.A.H., Kiegiel K., Isaacs R.J., Pickett J.S., Bowers K.E., Fierke C.A. *et al.* (2002) Photoaffinity analogues of farnesyl pyrophosphate transferable by protein farnesyl transferase. J Am Chem Soc;124:8206–8219.
25. Bikhtiyarov Y.E., Omer C.A., Allen C.M. (1995) Photoreactive analogues of prenyl diphosphates as inhibitors and probes of human protein farnesyltransferase and geranylgeranyltransferase type I. J Biol Chem;270:19035–19040.
26. Duckworth B.P., Xu J., Taton T.A., Guo A., Distefano M.D. (2006) Site-specific, covalent attachment of proteins to a solid surface. Bioconjug Chem;17:967–974.
27. Xu J., DeGraw A.J., Duckworth B.P., Lenevich S., Tann C.-M., Jenson E.C. *et al.* (2006) Synthesis and reactivity of 6,7-dihydrogeranylazides: reagents for primary azide incorporation into peptides and subsequent staudinger ligation. Chem Biol Drug Des;68:85–96.
28. Lee P.C., Petri R., Mijts B.N., Watts K.T., Schmidt-Dannert C. (2005) Directed evolution of Escherichia coli farnesyl diphosphate synthase (IspA) reveals novel structural determinants of chain length specificity. Metab Eng;7:18–26.
29. Agger S.A., Lopez-Gallego F., Hoye T.R., Schmidt-Dannert C. (2008) Identification of sesquiterpene synthases from Nostoc punctiforme PCC 73102 and Nostoc sp. strain PCC 7120. J Bacteriol;190:6084–6096.
30. Chowdhry V., Vaughan R., Westheimer F.H. (1976) 2-Diazo-3,3,3-trifluoropropionyl chloride: reagent for photoaffinity labeling. Proc Natl Acad Sci USA;73:1406–1408.
31. Turek T.C., Gaon I., Distefano M.D. (1997) Synthesis and rapid purification of 32P-labeled photoactive analogs of farnesyl pyrophosphate. J Labelled Comp Radiopharm;39:140–146.
32. Pompliano D.L., Gomez R.P., Anthony N.J. (1992) Intramolecular fluorescence enhancement: a continuous assay of ras farnesyl:protein transferase. J Am Chem Soc;114:7945–7946.
33. Bond P.D., Dolence J.M., Poulter C.D. (1995) A continuous fluorescence assay for protein:prenyl transferases. Meth Enzymol;250:30–43.
34. Bradford M.M. (1976) A rapid and sensitive method for the quantitation of microgram quantities of protein utilizing the principle of protein-dye binding. Anal Biochem;72:248–254.
35. Long S.B., Hancock P.J., Kral A.M., Hellinga H.W., Beese L.S. (2001) The crystal structure of human protein farnesyltransferase reveals the basis for inhibition by CaaX tetrapeptides and their mimetics. Proc Natl Acad Sci USA;98:12948–12953.
36. Strickland C.L., Weber P.C., Windsor W.T., Wu Z., Le H.V., Albanese M.M. *et al.* (1999) Tricyclic farnesyl protein transferase inhibitors: crystallographic and calorimetric studies of structure-activity relationships. J Med Chem;42:2125–2135.
37. Cramer F., Rittersdorf W., Boehm W. (1962) Chemistry of high-energy phosphates. XVIII. Synthesis of phosphoric acid esters and pyrophosphoric acid esters of the terpene alcohols. Annu Rev;654:180–188.
38. Cramer F., Weimann G. (1961) Imido esters. VII. Trichloroacetonitrile, a reagent for the selective esterification of phosphoric acid. Chem Ber;94:996–1007.
39. Umbreit M.A., Sharpless K.B. (1977) Allylic oxidation of olefins by catalytic and stoichiometric selenium dioxide with tert-butyl hydroperoxide. J Am Chem Soc;99:5526–5528.
40. Mitsunobu O., Wada M., Sano T. (1972) Stereospecific and stereoselective reactions. I. Preparation of amines from alcohols. J Am Chem Soc;94:679–680.
41. Mitsunobu O. (1981) The use of diethyl azodicarboxylate and triphenylphosphine in synthesis and transformation of natural products. Synthesis;1:1–28.
42. Turek T.C., Gaon I., Distefano M.D. (1997) Synthesis and rapid purification of 32P-labeled photoactive analogs of farnesyl pyrophosphate. J Labelled Comp Radiopharm;39:139–146.
43. Hahn K.M., Hastie S.B., Sundberg R.J. (1992) Synthesis and evaluation of 2-diazo-3,3,3-trifluopropanoyl derivatives of colchicine and podophyllotoxin as photoaffinity labels: reactivity, photochemistry, and tubulin binding. Photochem Photobiol;55:17–27.
44. Theodore L.J., Nelson W.L., Dave B., Giacomini J.C. (1990) Studies on Ca2+ channel antagonists. A 2-diazo-3,3,3-trifluoropropionamide derivative related to verapamil as a potential photoaffinity probe. J Med Chem;33:873–877.

45. Taylor J.S., Reid T.S., Terry K.L., Casey P.J., Beese L.S. (2003) Structure of mammalian protein geranylgeranyltransferase type-I. EMBO J;22:5963–5974.
46. Zhang H., Seabra M.C., Deisenhofer J. (2000) Crystal structure of Rab geranylgeranyltransferase at 2.0 A resolution. Structure;8:241–251.
47. Guo Z., Wu Y.-W., Das D., Delon C., Cramer J., Yu S. *et al.* (2008) Structures of RabGGTase-substrate/product complexes provide insights into the evolution of protein prenylation. EMBO J;27:2444–2456.
48. Krzysiak A.J., Rawat D.S., Scott S.A., Pais J.E., Handley M., Harrison M.L. *et al.* (2007) Combinatorial modulation of protein prenylation. ACS Chem Biol;2:385–389.
49. Hosokawa A., Wollack J.W., Zhang Z., Chen L., Barany G., Distefano M.D. (2007) Evaluation of an alkyne-containing analogue of farnesyl diphosphate as a dual substrate for protein-prenyltransferases. Int J Pept Res;13:345–354.
50. Chung J.A., Wollack J.W., Okesli A., Hovlid M.L., Chen Y., Mueller J.D. *et al.* (2009) Purification of prenylated proteins by affinity chromatography on cyclodextrin-modified agarose. Anal Biochem;386:1–8.
51. Long S.B., Casey P.J., Beese L.S. (2002) Reaction path of protein farnesyltransferase at atomic resolution. Nature;419: 645–650.
52. Dolence J.M., Cassidy P.B., Mathis J.R., Poulter C.D. (1995) Yeast protein farnesyltransferase: steady-state kinetic studies of substrate binding. Biochemistry;34:16687–16694.
53. Strickland C.L., Windsor W.T., Syto R., Wang L., Bond R., Wu Z. *et al.* (1998) Crystal structure of farnesyl protein transferase complexed with a CaaX peptide and farnesyl diphosphate analogue. Biochemistry;37:16601–16611.
54. Voelkert M., Uwai K., Tebbe A., Popkirova B., Wagner M., Kuhlmann J. *et al.* (2003) Synthesis and biological activity of photoactivatable N-ras peptides and proteins. J Am Chem Soc;125:12749–12758.
55. Alexander M., Gerauer M., Pechlivanis M., Popkirova B., Dvorsky R., Brunsveld L. *et al.* (2009) Mapping the isoprenoid binding pocket of PDEdelta by a semisynthetic, photoactivatable N-Ras lipoprotein. ChemBioChem;10:98–108.
56. Quellhorst G.J. Jr, Allen C.M., Wessling-Resnick M. (2001) Modification of Rab5 with a photoactivatable analog of geranylgeranyl diphosphate. J Biol Chem;276:40727–40733.
57. Wollack J.W., Zeliadt N.A., Mullen D.G., Amundson G., Geier S., Falkum S. *et al.* (2009) Multifunctional prenylated peptides for in vivo analysis. J Am Chem Soc;131:7293–7303.